L DWARFS AND THE SUBSTELLAR MASS FUNCTION

I. NEILL REID
Palomar Observatory, 105-24, California Institute of Technology, Pasadena, CA 91125; inr@astro.caltech.edu

J. DAVY KIRKPATRICK
Infrared Processing and Analysis Center, 100-22, California Institute of Technology, Pasadena, CA 91125

J. LIEBERT AND A. BURROWS
Steward Observatory, University of Arizona, Tucson, AZ 85721

J. E. GIZIS
Department of Physics and Astronomy, University of Massachusetts, Amherst, MA 01003

A. BURGASSER
Department of Physics, 103-33, California Institute of Technology, Pasadena, CA 91125

C. C. DAHN AND D. MONET
US Naval Observatory, P.O. Box 1149, Flagstaff, AZ 86002

R. CUTRI AND C. A. BEICHMAN
Infrared Processing and Analysis Center, 100-22, California Institute of Technology, Pasadena, CA 91125

AND

M. SKRUTSKIE
Department of Physics and Astronomy, University of Massachusetts, Amherst, MA 01003

ABSTRACT

Analysis of initial observations sky surveys has shown that the resulting photometric catalogs, combined with far-red optical data, provide an extremely effective method of finding isolated, very low-temperature objects in the general field. Follow-up observations have already identified more than 25 sources with temperatures cooler than the latest M dwarfs. A comparison with detailed model predictions (Burrows & Sharp 1999) indicates that these L dwarfs have effective temperatures between $\approx 2000 \pm 100$ K and 1500 ± 100 K, while the available trigonometric parallax data place their luminosities at between $10^{-3.5}$ and 10. Those properties, together with the detection of lithium in one-third of the objects, are consistent with the majority having substellar masses. The mass function cannot be derived directly, since only near-infrared photometry and spectral types are available for most sources, but we can incorporate VLM/brown dwarf models in simulations of the solar neighborhood population and constrain $\Psi(M)$ by comparing the predicted L dwarf surface densities and temperature distributions against observations from the Deep Near-Infrared Survey (DENIS) and 2 Micron All-Sky Survey (2MASS) surveys. The data, although sparse, can be represented by a power-law mass function, $\Psi(M) \propto M^{-\alpha}$, with $1 < \alpha < 2$. Current results favor a value nearer the lower limit. If $\alpha = 1.3$, then the local space density of $0.075 > M/M_\odot > 0.01$ brown dwarfs is 0.10 systems pc^{-3}. In that case, brown dwarfs are twice as common as main-sequence stars but contribute no more than $\sim 15\%$ of the total mass of the disk.

Subject headings: Galaxy: stellar content — stars: low-mass, brown dwarfs —
stars: luminosity function, mass function — stars: statistics

1. INTRODUCTION

The "stellar" mass function $\Psi(M)$ describes the final product of star formation, providing a global measurement of how diffuse gas is transformed into quasi-static spheres in thermal and hydrostatic equilibrium with masses from $\sim 100\ M_\odot$ to less than $0.1\ M_\odot$. The frequency of intermediate- and high-mass stars produced by this morphological restructuring determines galactic chemical evolution, while the proportion of material locked up in long-lived, low-luminosity dwarfs determines the overall mass-to-light ratio of a galactic population. It is the latter characteristic which, with the realization of the importance of dark matter (Ostriker & Peebles 1973), focused attention on Kumar's (1963) "black dwarfs": objects the central temperatures of which fail to cross the threshold for initiating hydrogen fusion. With luminous lifetimes that are brief in astronomical timescales, such objects might constitute substantial, but invisible, repositories of baryonic matter.

Relabeled as brown dwarfs (Tarter 1975), these "failed stars" have been the target of numerous surveys over the last two decades. Those projects reached fruition only in the last few years as substellar mass objects have been identified as stellar companions (Nakajima et al. 1995) in the Pleiades (Rebolo et al. 1995) and in the general field (Ruiz, Leggett, & Allard 1997; Tinney 1998). Until recently, however, statistical analyses have been hampered by the relatively small numbers of detected objects, particularly in the field where surveys were forced to rely on wide-field imaging at optical wavelengths. That circumstance has changed with the inception of the Deep Near-Infrared Survey (DENIS) (Epchtein et al. 1994) and 2 Micron All-Sky Survey (2MASS) (Skrutskie et al. 1997).

Very low mass (VLM) stars have effective temperatures of less than 3000 K, while brown dwarfs spend most of their lives at temperatures below 2000 K. As a result, the peak of the energy distribution lies at wavelengths in the 1–3 μm

region—where the only available large-scale survey is the pioneering Two Micron Sky Survey (Neugebauer & Leighton 1969)—which barely reaches the third magnitude in the K band. DENIS and 2MASS extend the sensitivity limits at near-infrared wavelengths by factors of more than 10^4 to $K_S \sim 13.5$ and $K_S \sim 15$ mag respectively (where K_S is the K-short passband defined by Persson et al. 1998). Both projects have succeeded in identifying extremely red, ultracool dwarfs (Delfosse et al. 1997; Kirkpatrick et al. 1999b, hereafter K2ML) with optical spectra similar to the previously known VLM dwarfs GD 165B (Kirkpatrick et al. 1999a) and Kelu 1 (Ruiz et al. 1997). Those sources clearly mark an extension of the M dwarf sequence to lower temperatures, and K2ML have codified that progression in defining the new spectral class, type L.

This paper uses new data provided by these surveys to probe the form of the mass function at and below the hydrogen-burning limit, comparing the DENIS and 2MASS observations against model predictions. Our analysis models the substellar mass function as a continuous extension of the stellar mass function, $\Psi_*(M)$: $M > 0.08\ M_\odot$. A prerequisite for those calculations, therefore, is an accurate description of $\Psi_*(M)$, serving as an anchor for our simulations. With that in mind, § 2 updates the census of stars and stellar systems within 8 pc of the Sun and defines $\Psi_*(M)$ in the range 0.1–1.0 $M_\odot$. Section 3 describes how theoretical predictions of $(L, T_{\rm eff})$ as a function of mass and age are matched against the $(K$ magnitude, spectral type) data for local L dwarfs; § 4 outlines the structure of the simulations; § 5 summarizes the results; and § 6 presents our conclusions.

2. THE STELLAR MASS FUNCTION

2.1. The Nearby Star Census

Until recently, most studies of the nearest stars followed van de Kamp (1972) in limiting the "solar neighborhood" to a 5.2 pc (17 lt-yr) radius sphere—a volume which encompasses only 45 stellar systems. The extensive surveys undertaken over the last three decades, notably spectroscopy of proper-motion stars and intensive radial velocity and high-resolution imaging searches for binary companions, allow present-day analyses to consider a larger sample—although one still restricted to declinations accessible from northern observatories (i.e., by Luyten at Palomar and Henry & McCarthy at Steward). Reid & Gizis (1997, hereafter RG97) laid the foundations of this reference sample, collating literature data for candidate nearby stars, particularly spectroscopy by Kirkpatrick, Henry, & Simons (1995) and Reid, Hawley, & Gizis (1995) of late-type stars from the (unpublished) preliminary version of the Third Nearby Star Catalogue compiled by H. Jahreiss and W. Gliese.

The RG97 nearby-star compilation lists 106 stellar systems, including 151 stars, which are both north of $\delta = -30°$ and, at the time of publication, had assigned distances of less than 8 pc from the Sun. The latter distances were based on a weighted combination of trigonometric parallax measurements and spectroscopic parallaxes. Completeness is clearly of paramount importance in these calculations, and RG97 present an extensive discussion of the available observations. They conclude that the sample is likely to be statistically complete at the $\sim 90\%$ level. In particular, they note that while an extrapolation of the 5.2 pc luminosity function predicts ~ 30 additional $r < 8$ pc mid–type M dwarfs, all would be expected to have $m_r < 16$,

well above the magnitude limit of available proper-motion catalogs. Nonetheless, since this marks the first attempt to extend coverage to these larger distances, one expects modifications to the sample as new, more accurate data are obtained. The *Hipparcos* astrometric catalog (ESA 1997) provides such observations for many systems in the initial 8 pc sample, while more detailed searches for binary (and tertiary) companions have also been undertaken. We have used these new results to produce a revised northern 8 pc catalog as our baseline sample.

Hipparcos measurements eliminate four single stars and two binaries from the RG97 8 pc sample. Two other binaries, Gl 185 and Gl 831, are formally outwith the 8 pc limit, if one adopts the *Hipparcos* parallaxes outright, but lie just within the limit in a weighted combination of ground-based and *Hipparcos* data. Of the 108 stars in 100 systems with *Hipparcos* parallaxes $\pi_H > 0.''125$, 18 are south of $\delta = -30°$ and five are northern stars with parallax measurements of low precision.[1] Those stars are not included in the present analysis. However, the improved *Hipparcos* astrometry adds several confirmed M dwarfs to the 8 pc sample, each with parallax measured to milliarcsecond precision. Table 1 summarizes the resultant additions and subtractions.

Newly discovered binary and tertiary companions further modify the sample. Delfosse et al. (1999a) have identified additional components in three of the systems listed in RG97 (Table 1), while Henry et al. (1997, 1999) and Oppenheimer et al. (1999) use higher resolution imaging to identify new members in five systems (two in common with Delfosse et al.). These new discoveries eliminate two stars from the sample: LP 476-407 was resolved as a visual binary by Henry et al.'s (1997) speckle imaging, and the primary component is a double-lined spectroscopic binary (Delfosse et al. 1999a), while infrared speckle measurements show that G89-32 is an equal-luminosity binary, with a separation of $0.''7$ (Henry et al. 1997). In both cases the fainter apparent magnitude of each component leads to a smaller inferred spectroscopic parallax, removing the systems beyond the 8 pc limit.

The other four systems with newly discovered companions remain within the 8 pc sample since all have trigonometric parallax measurements. Gl 831 and Gl 896 were identified previously as binaries, while RG97 list Gl 829 as a single star. Henry et al. and Delfosse et al. have discovered one new companion in each, reclassifying the systems as two triples and a binary respectively.[2] Finally, Oppenheimer et al.'s observations have revealed a third component in the LTT 1445 (LP 771-95/96) system.

Including both the brown dwarf Gl 229B and the Sun, the revised northern 8 pc catalog includes 150 objects in 103 systems: 68 single stars, 25 binaries, nine triples and one quadruple.[3] All but four systems have distances derived from accurate trigonometric parallax measurements, with

---

[1] The five stars in question are BD $-13°637$B, Gl563.2A and B, BD $+24°3192$B, and BD $-15°6346$B. Spectroscopy with the Double Spectrograph on the Hale 200 inch (5.08 m) telescope identifies all five as K-type stars—clearly incompatible with the $M_V > 12.5$ inferred from π_H.

[2] Delfosse et al. (1999a) also show that the previously known companion in the SB1 binary G203−47 is a white dwarf; thus, there is a total of nine degenerates in the sample—four single stars and five companions.

[3] RG 97 considered Gl 643/Gl 644 as a quintuple, but *Hipparcos* astrometry shows that Gl 643 is nearer by 0.75 pc. Given this substantial separation, we group the five stars as a single and a quadruple system.

TABLE 1

REVISIONS TO THE REID/GIZIS (1997) NORTHERN 8 PARSEC SAMPLE

Name	M_V	$(B-V)$	$(V-I)$	HIP	π	Comments
			Rejected Stars			
Gl 178	3.67	0.46	0.52	22449	0.1246 ± 0.0010	*Hipparcos* π
Gl 190	10.45	1.53	2.64	23932	0.1073 ± 0.0020	*Hipparcos* π
Gl 623A	10.98	1.50	2.30	80346	0.1243 ± 0.0016	*Hipparcos* π
Gl 623B	16.04	...	...	...	...	
Gl 686	10.07	1.53	2.11	86287	0.1230 ± 0.0016	*Hipparcos* π
Gl 713A	4.04	0.49	...	89937	0.1241 ± 0.0005	*Hipparcos* π
Gl 713B	4.65	...	...	...	...	
LP 476-207AabB	13	...	...	...	0.11 ± 0.03	New component,[a,b] $\pi_{\rm spec}$
G89-32AB	13	...	...	...	0.10 ± 0.03	New component,[a] $\pi_{\rm spec}$
			Additional Stars			
Gl 382	9.80	1.50	2.17	49986	0.1280 ± 0.0015	*Hipparcos* π
Gl 701	9.91	1.50	2.06	88574	0.1283 ± 0.0014	*Hipparcos* π
LP 816-60	12.7	...	...	103039	0.1822 ± 0.0037	*Hipparcos* π
Gl 793	11.05	1.56	2.43	101180	0.1256 ± 0.0011	*Hipparcos* π
Gl 829B	11.9	...	...	106106	0.1483 ± 0.0019	New component[b]
Gl 831C	15.4	...	...	...	0.126 ± 0.023	New component[a]
Gl 896Aa	~13	...	...	116132	0.1601 ± 0.0028	New component[b,c]
LTT 1445C	~14.5	...	...	...	0.127 ± 0.025	New component,[c] $\pi_{\rm spec}$

NOTES.—The first group of stars listed are rejected because the *Hipparcos* parallax is less than 0″.125. LP 476-207 and G89-32 are eliminated due to the smaller inferred spectroscopic parallax. Additions to the 8 pc sample stem either from improved parallax data from the *Hipparcos* satellite or from new discoveries in surveys for multiple stars.

[a] Henry et al. 1997.

[b] Delfosse et al. 1999a.

[c] Oppenheimer et al. 1999—LTT 1445 = LP 771-95/96 (RG97).

68 based on *Hipparcos* data. The overall multiple star fraction (i.e., the fraction of stellar systems that consist of two or more starlike objects) is 34.0%, while the companion star frequency (or the number of pairs) is 44.7%. Both values are very close to those derived by RG97.

2.2. *The Mass-Luminosity Relation*

Computing the stellar mass function from these data demands that we adopt a mass-luminosity relation. RG97 derived mass functions for their 8 pc sample using Henry & McCarthy's (1993, hereafter HMc93) empirical (mass, M_K) relation, Kroupa, Tout, & Gilmore's (1993) relation, and theoretical calibrations by Burrows et al. (1993) and Baraffe & Chabrier (1996).[4] The results are in good agreement, save for the calibration based on the $(M_{\rm bol}, {\rm mass})$ relation predicted by the last-mentioned set of models. On that basis, RG97 adopted the HMc93 empirical relation, derived from astrometric orbit analysis or nearby stars, as their standard.

Baraffe et al. (1998, hereafter BCAH98) present color-magnitude and mass-luminosity relations for a revised set of solar-abundance models, and Figure 1 (*top*) compares their predictions for ages of 0.1, 1, and 10 Gyr against both the HMc93 calibration and available measurements of stellar masses.[5] Astrometric orbital determinations are supplemented by data for eclipsing binaries as summarized by Andersen (1991), including YY Geminorum; analysis of the well-known M4.5 binary CM Draconis (Metcalfe et al. 1996);[6] and data for the recently discovered mid-M eclips-

ing system, GJ 2069A (Delfosse et al. 1999b). We have estimated M_K for both components in the last system based on the absolute visual magnitudes listed by Delfosse et al. and the $(M_V, (V-K))$ relation for nearby stars. Those estimates, to which we assign generous uncertainties of ±0.2 mag, are consistent with values based on the spectral type. Both stars are subluminous by ~1 mag as compared with the theoretical and empirical calibrations, as expected given the discrepancies noted by Delfosse et al. at visual wavelengths, and adding to the already substantial dispersion in the diagram for $1.0 > M/M_\odot > 0.3$. There is no evidence that the system is metal poor based on the CaH and TiO band strengths (Reid et al. 1995). Moreover, the discrepancy is not restricted to astrometric binaries: GJ 2069Ab has similar photometric properties to the CM Dra components but almost twice the mass. Clearly stars in this mass range, and GJ 2069Aab in particular, require more attention, but for the present we must assume that we can derive a valid mass-luminosity relation for the average disk dwarf.

The location of the mean mass-luminosity relation is predicted to vary as a function of age and abundance, while the detailed shape is tied to the underlying stellar physics, notably H_2 dissociation at ~0.7 $M_\odot$ (Copeland, Jensen, & Jorgensen 1970) and the onset of degeneracy below 0.15 $M_\odot$ (Grossman 1970). D'Antona & Mazzitelli (1985) originally emphasized the potential for systematic errors if $\Psi(M)$ is derived by applying simplified mass-luminosity relations to luminosity function data. The importance of changes of slope in (L, M) depends on the number of stars at the relevant luminosities. Rather than bin the data to give $\Phi(M_K)$, we plot the distribution of the 8 pc sample in the M_K versus r^3 plane (where r is the distance) in Figure 1b. This diagram permits a visual assessment of both the number density of stars near points of inflection in the (L, M) relation and of

---

[4] Note that RG97 calculations are made on a star-by-star basis, not via a calculation of the nearby-star luminosity function.

[5] The "kink" in the empirical relation at 0.5 $M_\odot$ reflects its origins as two linear relations in the $(M_K, \log M)$-plane.
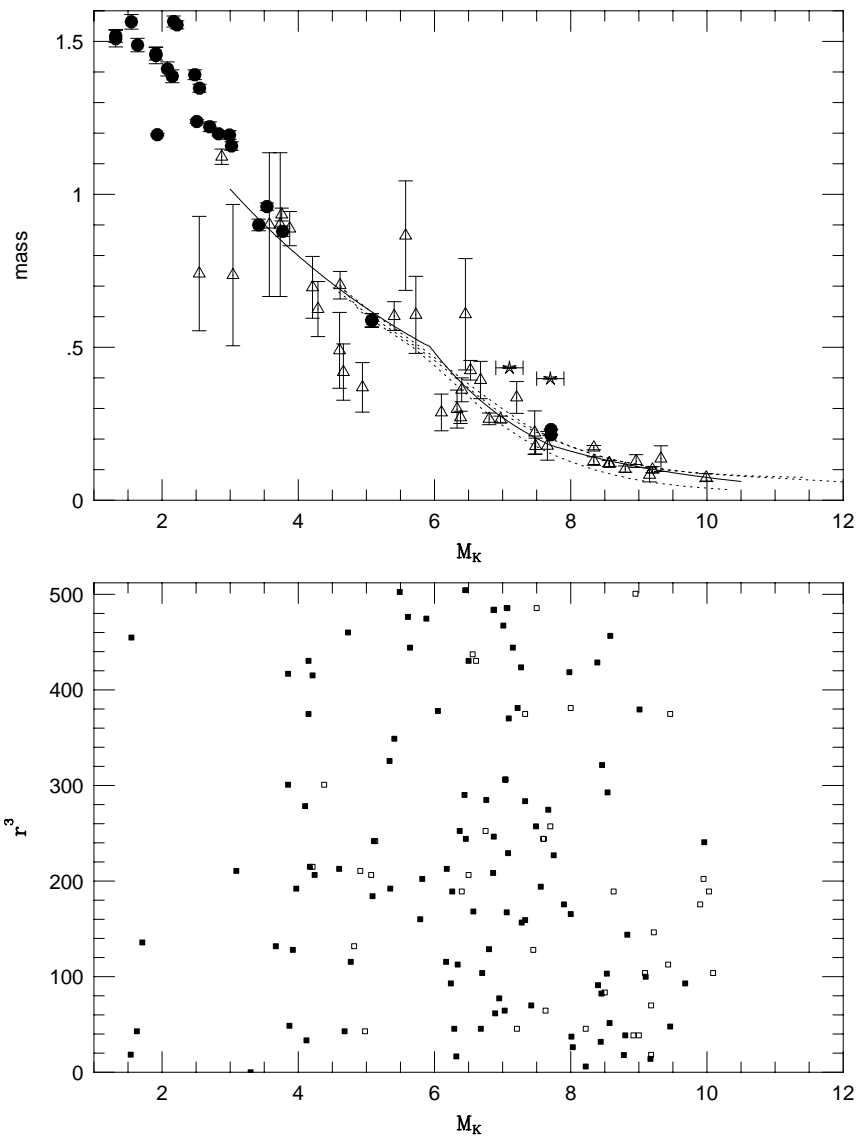
[6] CM Draconis is misplotted in Fig. 2 of Reid (1998).

FIG. 1.—(*Top*): (M_K, mass) relation: solid points are eclipsing binaries; open triangles are from Henry & McCarthy (1993). The solid line is the empirical relation from the latter paper, while the dotted lines are theoretical relations from Baraffe et al. (1998) for ages of 0.1, 1 and 10 Gyr. (*Bottom*): The distribution of the 8 pc stars in the (r^3, M_K) plane. Solid points mark the brightest stars in individual systems.

the completeness of the sample as a function of distance. The distribution of points suggests a scarcity of very low mass M dwarfs, $M_K > 9$, beyond ~ 6 pc.

Both the range of chemical abundances and the age distribution of the calibrating stars can influence the derivation of $\Psi(M)$ by biasing the derived (mass, M_K) relation. In the former case, the contribution to the dispersion in derived masses is likely to be small, since *Hipparcos* color-magnitude data indicate that $\sim 90\%$ of disk dwarfs have metallicities in the range $-0.3 < [\mathrm{M/H}] < 0.1$ (Reid 1999). Moreover, our choice of M_K in calibrating masses should minimize metallicity variations.

Age variations are likely to affect only the lowest masses. The BCAH98 isochrones plotted in Figure 1 show no evidence for significant evolution in M_K between the ages of 1 and 10 Gyr but indicate that very low mass ($<0.1~M_\odot$) dwarfs can be up to 1 mag brighter in K at age 0.1 Gyr than at 1 Gyr. There have been suggestions that the binary stars observed by HMc93 are biased toward younger ages, most recently by Chabrier & Baraffe (1998). Almost all of those

proposals are based on the detection of chromospheric and/or coronal activity among the lower-luminosity dwarfs in the HMc93 sample, and all are based on a misconception. Chromospheric activity in M dwarfs is a function of *both* age and mass and persists for several Gyr in mid- and late-type dwarfs. Hawley, Gizis, & Reid (1996) have compiled statistics of activity as a function of type and show that over 50% of dwarfs with spectral types of M5.5 or later are dMe stars; Hawley, Reid, & Tourtellot (1999) have detected emission in an M5 dwarf in the 5 Gyr old cluster M67; and, of particular relevance in this case, fully 80% of the 2MASS M7–M9 dwarfs with spectroscopic observations have substantial (>5 Å equivalent width) emission (Gizis et al. 1999). Thus, activity among the lowest luminosity dwarfs is expected and cannot be taken as a sign of youthfulness.

Chabrier & Baraffe (1998) comment that the three lowest mass HMc93 dwarfs are overluminous compared with their model predictions, again interpreting this as a sign of youthfulness. However, they explicitly plot the three dwarfs with the lowest measured masses. A symmetric distribution of

observational errors demands that those objects will also be overluminous. The full set of low-mass dwarfs is well distributed about the mean relation plotted in Figure 1, and similar circumstances prevail for the extended sample of low-mass binary components with orbits and mass determinations derived from *HST* FGS observations (Henry et al. 1999). The (mass, M_V) relation defined by those stars is identical to that deduced by Henry & McCarthy (1993). Since in toto these stars represent essentially all of the local binary systems accessible to astrometric observations, an unbiased sample, this internal consistency argues strongly that all lie close to their main-sequence configuration.

2.3. The Mass Function

Defining our terminology, the stellar mass function is written as

$$\Psi(M) = \frac{dN}{dM} \text{ stars per unit mass.}$$

Following Salpeter's (1956) pioneering analysis, the mass function is often expressed as a power law. In that case it is useful to define

$$\xi(M) = \frac{dN}{d \log M} \text{ stars per unit log mass .}$$

A power-law mass function $\Psi(M) \propto M^{-\alpha}$ corresponds to $\xi(M) \propto M^{-\alpha+1}$, also written as $\xi(M) \propto M^{\Gamma}$ (see Scalo 1998). This formulation provides a convenient way of representing $\Psi(M)$, which we adopt in this paper. This should not be misinterpreted as a statement that $\Psi(M)$ *is* a power law.

Figure 2 shows mass functions derived from data for the revised 8 pc sample using both the empirical calibration and the BCAH98 1 Gyr isochrone [adopting the 10 Gyr isochrone does not change $\Psi(M)$ in any significant fashion]. White dwarfs are excluded. The two calibrations give results in good agreement, with the empirical relation giving a somewhat larger spread in mass below 0.1 $M_\odot$. For present purposes, we are concerned with the general form of the mass distribution rather than assessing whether any indications of structure have statistical weight (the individual uncertainties argue against that proposition) and fit a simple power law over the 1.0–0.1 $M_\odot$ mass range. The best-fit relations are

$$\log \xi_*(\log M) = -0.13 \pm 0.14 \log M + 1.02 \pm 0.08$$

for the empirical (HMc93) calibration, and

$$\log \xi_*(\log M) = 0.02 \pm 0.14 \log M + 1.10 \pm 0.08$$

for the BCAH98 (mass, M_K) relation. In these equations, M is the mass in solar masses and the units are the number of stars per $0.1 \log M$ within the volume of the northern 8 pc sample (1608 pc^{-3}). These relations correspond to mass functions $\Psi_*(M) \propto M^{-1.13\pm0.14}$ and $\Psi_*(M) \propto M^{-0.98\pm0.14}$, respectively, and a space density of 0.035 stars pc^{-3} (0.1 $M_\odot$)$^{-1}$ at $M = 0.1 M_\odot$.

Nearly one-third of the main-sequence dwarfs included in the star-by-star mass function are companions of more massive stars. Excluding those stars (i.e., limiting the sample to single stars and primaries in multiple systems) gives the mass functions plotted as dotted lines in Figure 2. These are determinations of the systemic mass function, $\Psi_{sys}(M) \propto M^{-0.92\pm0.13}$ from HMc93, and $\Psi_{sys}(M) \propto M^{-0.89\pm0.13}$ based on the BCAH98 models. The corresponding space
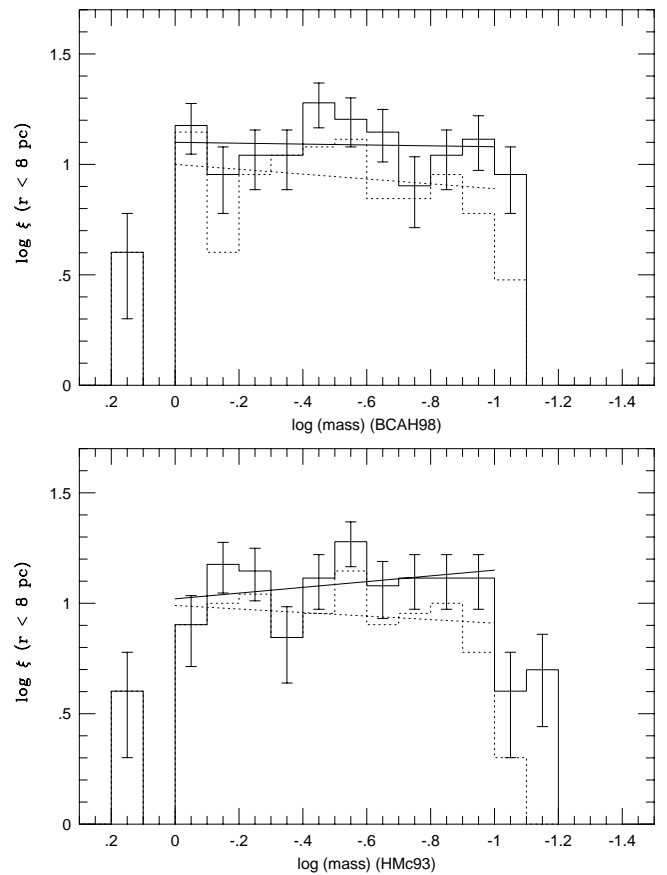

FIG. 2.—Stellar mass function defined by the northern 8 pc sample. The upper diagram plots the results if we adopt the empirical HMc93 calibration; the lower for masses calibrated by the 1 Gyr BCAH98 isochrone. In both cases the solid histogram/line delineates the star-by-star function; the dotted line marks the systemic function.

density of stellar systems at 0.1 $M_\odot$ is 0.02 systems pc^{-3} (0.1 $M_\odot$)$^{-1}$, or ~60% of the star-by-star space density. In the simulations described in the following sections, the reference is set by the mean density of stellar systems, rather than by individual stars, in the 0.1–1 $M_\odot$ mass range.

3. MODELING THE LOCAL SPACE DENSITY OF BROWN DWARFS

An accurate determination of $\Psi_*(M)$ at masses below 0.15 $M_\odot$ is rendered difficult by the low intrinsic luminosity of VLM dwarfs and the consequent difficulties involved in finding such stars in even the immediate vicinity of the Sun. VLM dwarfs, however, at least achieve a stable, long-lived configuration in (log L, T_{eff}), defining the main sequence in the H-R diagram and leading to mass-luminosity and mass-effective temperature relations which are effectively single-valued (see Fig. 1). The latter situation does not prevail for brown dwarfs, which descend rapidly through the H-R diagram with $L \propto M^{2.6} t^{-1.3}$ and $T_{eff} \propto M^{0.8} t^{-0.3}$ (Burrows & Liebert 1993). All substellar-mass objects evolve through at least part of the L dwarf sequence, albeit at very different rates. Consequently, one cannot associate a given spectral type (or luminosity) with a specific mass. Instead, we can only constrain $\Psi(M)$ at masses below 0.08 $M_\odot$ by comparing the overall distribution of the observed characteristics against predictions based on theoretical simulations.

Evolutionary models of low-mass stars and brown dwarfs constitute the backbone of our simulations. The two most recent sets of such models are by Burrows et al. (1997), who extend the calculations undertaken by Burrows et al. (1993) and by Baraffe et al. (1998). The former set takes account of opacities due to dust grains, which are predicted to form at temperatures below ~ 2400 K, but use gray atmospheres to define the outer boundary conditions; the latter employ the latest model atmospheres computed by Allard & Hauschildt, but include no grain opacities. Both predict similar isochrones, as Figure 3 shows, with differences of only 100–200 K at stellar masses. The Baraffe et al. models predict similar luminosities but lower temperatures for young- and intermediate-age low-mass stars and higher luminosities and higher temperatures at substellar masses (and for $M \leq 0.08\ M_\odot$ at age 10 Gyr). Given that we are concerned primarily with the latter low-mass range, where grains make a substantial contribution to the overall opacity and temperature structure, we have taken the Burrows et al. models as the reference for the current analysis.

Having chosen a reference set of isochrones, our aim is to model the 2MASS and DENIS L dwarfs—magnitude-limited samples are drawn from several hundred square degree areas. We have measurements of near-infrared apparent magnitudes IJK_S (DENIS) and $iJHK_S$ (2MASS, where i is determined from Keck spectra; see K2ML) and spectral types for each object but direct distance determination for only a handful. In contrast, the stellar models predict intrinsic luminosity and effective temperature as a function of mass and age. Given that our goal is to match both the number of L dwarfs detected and the spectral type distribution of those L dwarfs, we require the following: first, estimates of the stellar birthrate, $B(t)$, and the initial mass function, $\Psi(M)$, to predict the local space density of low-temperature dwarfs; second, an estimate of the K-band bolometric corrections to transform $\log L$ to M_K and predict the number of sources detected by 2MASS; and, third, a relation between effective temperature and spectral type, to estimate the distribution of detected sources. None of these relations is well established observationally. However, the approximate L dwarf effective temperature scale outlined in K2ML provides the basis for a preliminary analysis of this issue.

3.1. The Spectral Type/Effective Temperature Relation

Effective temperature calibration for late-type dwarfs has been a subject of some debate for well over a decade. Different analysis techniques have produced temperature scales which disagree by 300 K or more at spectral types later than M7. Blackbody fitting to broadband photometry, originally applied by Greenstein, Neugebauer, & Becklin (1970), generally leads to the coolest temperature estimates, while near-infrared and optical spectroscopic analyses, matched against stellar models, give progressively hotter scales. Thus, temperature estimates for the well-known M8 dwarf VB 10 have ranged from ~ 2330 K (Tinney, Mould, & Reid 1993a—blackbody fitting) to ~ 2750 K (Jones et al. 1995—
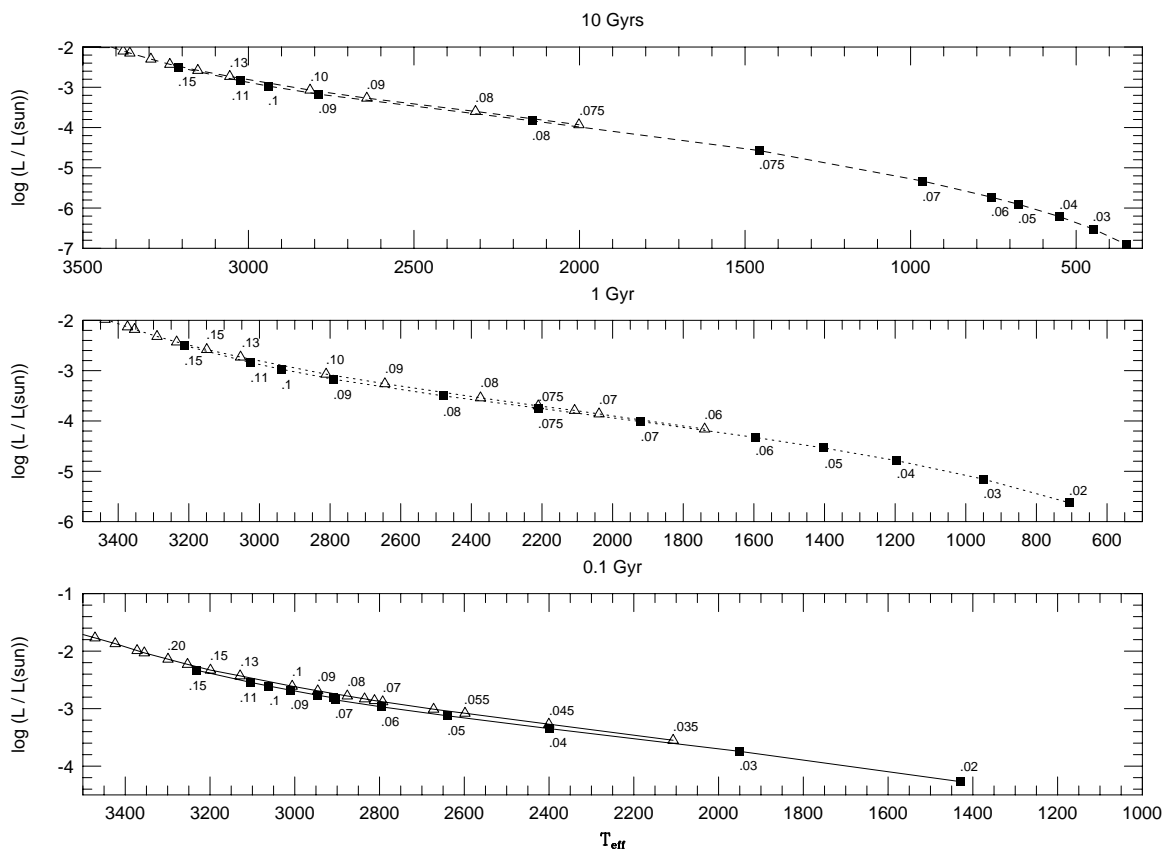

FIG. 3.—Comparison between the Burrows et al. (1993, 1997) (*filled squares*) and Baraffe et al. (1998) models (*open triangles*) in the (log II L, T_{eff})-plane. The Burrows et al. data are plotted for masses of 0.02, 0.03, 0.04, 0.05, 0.06, 0.07, 0.075, 0.08, 0.09, 0.1, 0.11, and 0.15 $M_\odot$; the Baraffe et al. data points are for masses of 0.035, 0.045, 0.05, 0.06, 0.070, 0.072, 0.075, 0.08, 0.09, 0.10, 0.13, 0.15, 0.175, 0.20 $M_\odot$ (0.1 Gyr); 0.06 $M_\odot$ et seq. for 1 Gyr; and 0.075 $M_\odot$ et seq. for 10 Gyr.

near-infrared spectra) and ~ 2875 K (Kirkpatrick et al. 1993—optical and near-infrared spectra).

Recent theoretical analyses have identified a different method of temperature determination. Tsuji, Ohnaka, & Aoki (1996a) originally suggested that dust grains, long known to be present in the low-density atmospheres of asymptotic giant branch stars, should also form in cool main-sequence dwarfs. Dust formation depletes the gas-phase population of a number of molecular species, leading to significant changes in the emergent spectrum, notably the weakening and subsequent disappearance of TiO and VO absorption. It is now clear that this process is responsible for the hydride-dominated optical spectra of L dwarfs.

Tsuji et al. (1996b) and Jones & Tsuji (1997) have computed model atmospheres which include TiO depletion and find that these "dusty" models give much improved agreement between the predicted and observed depths of the near-infrared water bands in late-type M dwarfs. Their temperature estimates of ~ 2600 K for Gl 406 (M6), ~ 2200 K for VB 10, and ~ 2000–2200 K for LHS 2924 (M9) are comparable to blackbody scales, even though the overall energy distributions of both late-type M dwarfs and L dwarfs are far from Planck curves. Nonetheless, Tinney et al. (1993a), anchoring their blackbody curves using L-band (3.4 μm) photometry, estimated $T_{\rm eff} \sim 2080$ K for LHS 2924 and $T_{\rm eff} \sim 2600$ K for Gl 406.

Burrows & Sharp (1999) have extended grain condensation calculations to include a wider range of molecular species, and K2ML demonstrate that there is broad agreement between theoretical calculations of the expected appearance and disappearance of different molecules with decreasing temperature and the observed progression of band strengths in the L dwarf sequence. Detailed analyses lead to temperature estimates of ~ 1900 K for the L2 dwarf Kelu 1 (Ruiz et al. 1997), and 1800–1900 K for the L4 dwarf GD 165B (Tsuji et al. 1996b; Kirkpatrick et al. 1999a). The decreasing strength of CrH and, perhaps, Li I, together with the absence of the 2.2 μm band due to CH_4, suggest a temperature of between 1400 and 1500 K for the coolest known L dwarf 2MASS J1632291+190441 (type L8).

Combining these results, we derive the approximate temperature scale plotted in Figure 4. The L dwarf sequence is characterized as lying between effective temperatures of 2000 K (type L0/L1) and ~ 1400 K (i.e., somewhat cooler than spectral type L8). It is likely that there is some overlap between L0/L1 dwarfs and the latest M dwarfs in the 2000–2100 K temperature range. There are obviously appreciable uncertainties both in the boundary values we adopt and in the overall scale, and those uncertainties are taken into account in the analysis of the simulations described in the following section.

3.2. K-Band Bolometric Corrections for L Dwarfs

Transforming bolometric luminosities to M_K magnitudes is a relatively straightforward process. Figure 5 plots BC_K, where

$$BC_K = M_K - M_{\rm bol}$$

acts as a function of effective temperature (using the scale defined in the previous subsection) for a number of well-known dwarfs. As yet, GD 165B and Gl 229B are the only ultracool dwarfs with flux measurements at wavelengths longward of 2.2 μm. However, the peak in the emergent spectral energy distribution lies close to the K band over
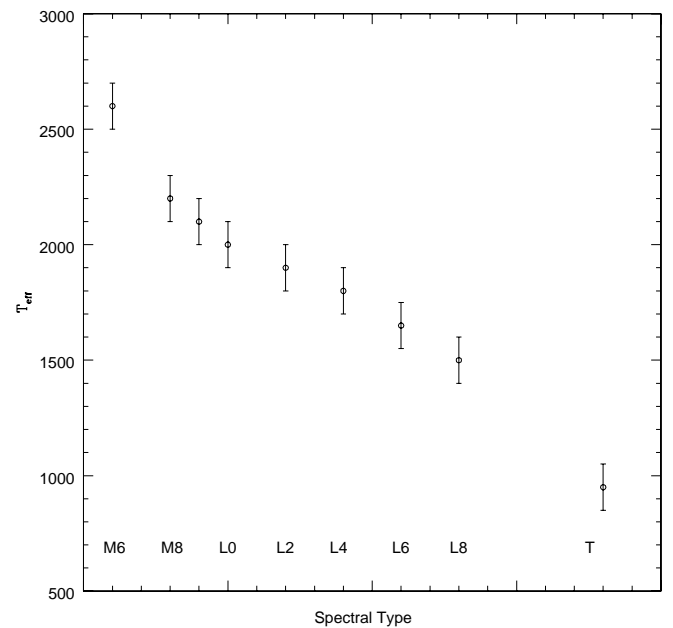

Fig. 4.—Effective temperature/spectral type relation adopted in this paper.

this range in temperature and little variation is expected in the value of BC_K from spectral type $\sim$M4 through L4 (GD 165B) to $\sim$L8. At some temperature between the latter spectral type and the ~ 950 K measured for Gl 229B, methane becomes a significant absorber at near-infrared wavelengths, removing $\sim 60\%$ of the flux emitted in the K passband. Burrows & Sharp (1999) place this transition at a temperature between 1500 and 1200 K. To date, no brown dwarfs have been discovered with properties intermediate between those of 2MASS J1632291+190441, which has no significant methane absorption at 2.2 μm, and the lone T dwarf, Gl 229B, so it remains unclear both exactly where methane absorption becomes important and whether the onset is gradual or abrupt.

The shape of the L/T transition in the (BC_K, $T_{\rm eff}$) plane affects predictions of both the color distribution and the expected total numbers of detectable brown dwarfs with $T_{\rm eff} < 1400$ K. Increasing BC_K at a given temperature implies a fainter M_K and hence a smaller spatial volume accessible to a magnitude-limited survey. At the same time, an increased BC_K leads to bluer ($J-K$) colors, since the J passband is unaffected by CH_4 absorption [$BC_K \sim -3$ corresponds to ($J-K$) ~ 1.0]. We have explored the different possibilities to a limited extent by considering two ad hoc relations: an abrupt decrease in BC_K of 1.3 mag between temperatures of 1400 and 1300 K (relation A in Fig. 5) and a similarly sharp transition between 1200 and 1100 K (relation B). These are chosen to span the theoretically predicted temperature range for the onset of substantial methane absorption. Relation B predicts larger numbers of L dwarfs to a given apparent magnitude limit but fewer 2MASS-detectable brown dwarfs with intermediate or blue ($J-K$) colors.

3.3. The Stellar Birthrate and $\Psi(M)$

The temperature distribution of brown dwarfs in the solar neighborhood depends on both the mass and the age distribution and is therefore tied directly to the convolution of $B(t)$ and $\Psi(M)$. However, the currently available obser-
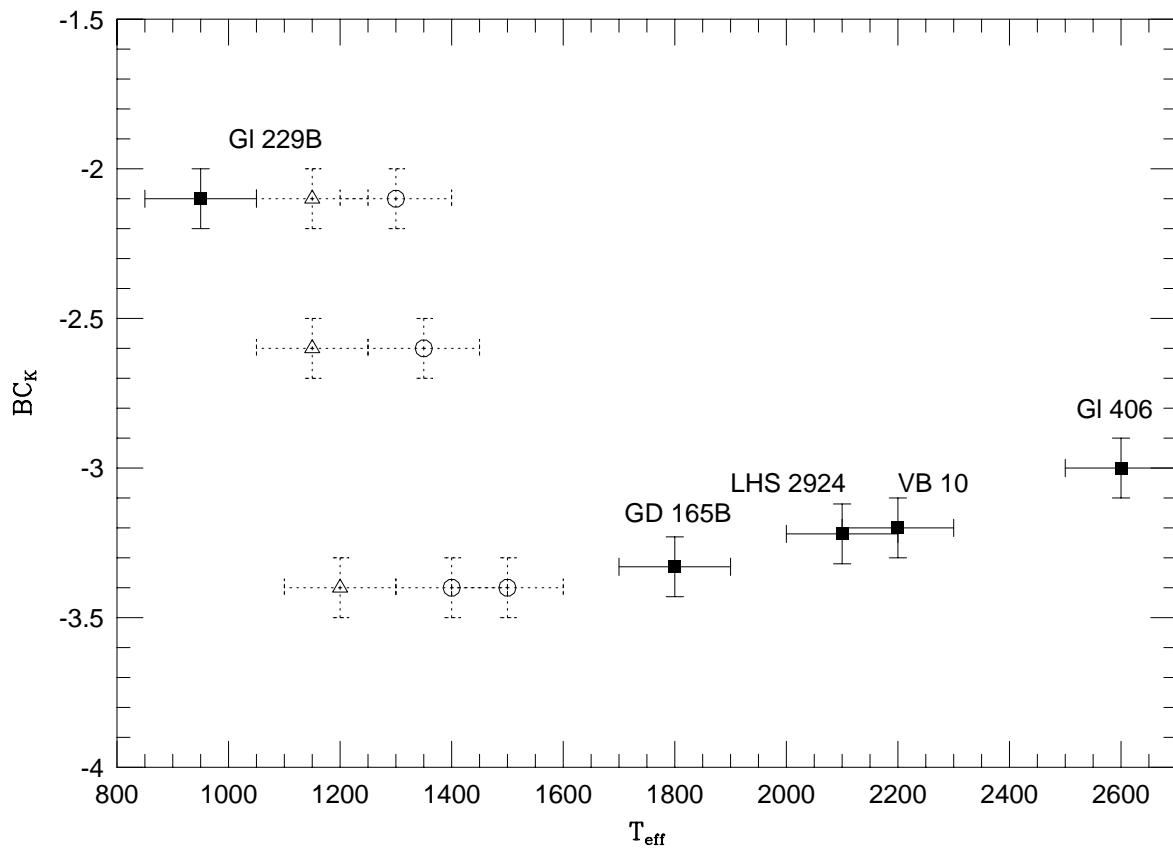
Fig. 5.—K-band bolometric corrections as a function of temperature. The solid points are measured bolometric corrections by Tinney et al. (1993a; Gl 406, VB10, LHS 2924, and GD 165B) and Matthews et al. (1996; Gl 229B). The open symbols outline the two relations adopted in our simulations to estimate the variation in BC_K with the onset of CH_4 absorption: relation A is identified by open circles, relation B by open triangles.

vations do not allow us to separate the two functions. Figure 6 shows the predicted evolution of effective temperature as a function of time for objects with masses between 0.009 and 0.1 $M_\odot$. As discussed by Burrows et al. (1997), objects segregate into two well-defined categories: those sufficiently massive to ignite central hydrogen burning and achieve a stable, main-sequence configuration with a near-constant effective temperature, $M \geq 0.08\ M_\odot$; and brown dwarfs, $M < 0.07\ M_\odot$, which show monotonic decrease in T_{eff}, after an initial deuterium phase for $M \geq 0.015\ M_\odot$. VLM dwarfs with masses between ~ 0.075 and 0.08 $M_\odot$ are transition objects, which maintain near-constant T_{eff} for a substantial fraction of a Hubble time.

Our best estimate of the L dwarf domain, $2000 > T_{eff} > 1400$ K, is indicated in Figure 6. Given those temperature limits, M9 dwarfs such as LHS 2924 and BRI 0021 are predicted to have masses of $\sim 0.08\ M_\odot$, with L0 dwarfs slightly less massive. Thus, based on the Burrows et al. (1993, 1997) evolutionary tracks, the only stars expected to enter the L dwarf regime are those within $\sim 0.04\ M_\odot$ of the hydrogen-burning limit. All other L dwarfs are brown dwarfs.

Figure 6 illustrates an important characteristic of the L dwarf population: since L dwarfs are defined by the effective temperature, our sample (indeed any sample) includes transition objects and brown dwarfs which span a wide range of age and exhibit little overlap in the age distribution at different masses. As an extreme example, while a 0.075 $M_\odot$ brown dwarf enters the L dwarf regime at an age of ~ 1.25 Gyr and cools to 1400 K at age ~ 10 Gyr, a 0.009 $M_\odot$

object has a spectral type of L0 at age 3 Myr and L9 at age 12 Myr. This has two important consequences: first, higher mass brown dwarfs and VLM stars make a proportionately larger contribution to the L dwarf population—indeed, given the absence of star formation in the immediate vicinity of the solar neighborhood and the limiting magnitude of 2MASS, there is very little chance of our identifying any free-floating brown dwarfs below 0.015 $M_\odot$; second, short-term variations in the star formation rate can mimic changes in the slope of the initial mass function—and, conversely, we cannot infer $B(t)$ from these data without making assumptions about $\Psi(M)$.

Other methods can be used to estimate $B(t)$ for the Galactic disk, notably the distribution of chromospheric activity in the local stellar population. These analyses are complicated to some extent by likely variations in the activity of individual stars, such as the Maunder minimum phenomenon in solar-type dwarfs. However, Soderblom, Duncan, & Johnson (1991) have demonstrated that the available data for G dwarfs and M dwarfs are consistent with a uniform star formation rate over the past 9 Gyr. Henry, Soderblom, & Donahue (1996) have extended the observational sample to include some 800 G-type southern stars and to confirm the distribution of activity deduced from the northern samples. Noh & Scalo (1990) have used the white dwarf luminosity function to probe the star formation history and find some indications of increased activity within the last 10^9 years, although the evidence is not conclusive. Given these circumstances, we assume a uniform star formation rate in the present simulations.
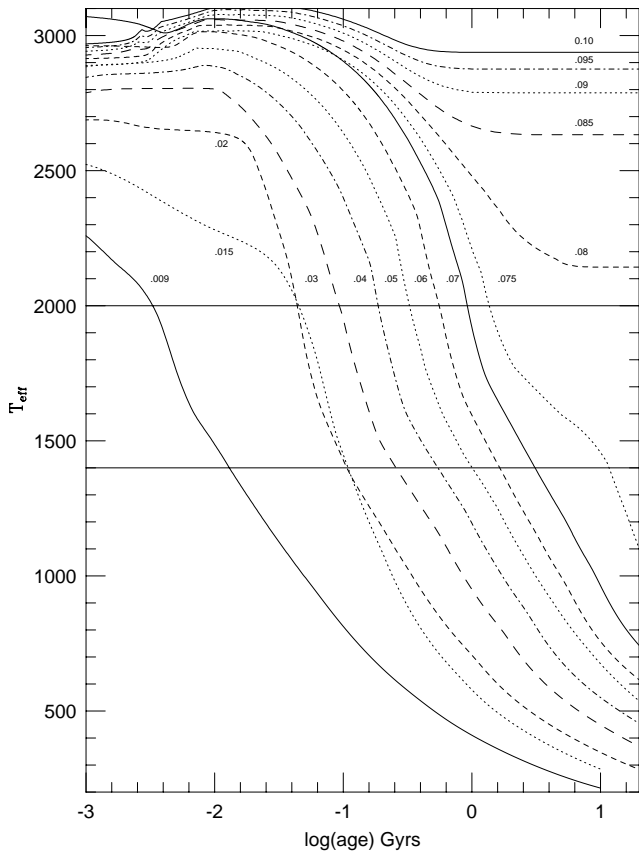
FIG. 6.—Effective temperature/age relation defined by the Burrows et al. (1997, 1993) models. The evolutionary tracks are plotted for masses of between 0.009 and 0.10 $M_\odot$, with the individual curves identified on the diagram. The horizontal lines outline the temperature range which corresponds to the L dwarf spectral type.

FIG. 7.—H-R diagram from VLM/brown dwarfs: we plot Burrows et al. (1993, 1997) models for masses of 0.015, 0.03, 0.05, 0.06, 0.07, 0.08, 0.09, and 0.1 $M_\odot$; the lowest-mass track lies at the highest luminosity at a given temperature. The solid points indicate the positions of the VLM dwarfs Gl 406, VB10, and LHS 2924; the open circles mark the four L dwarfs with trigonometric parallax measurements. The uncertainties in luminosity are primarily due to uncertainties in the bolometric corrections.

3.4. The H-R Diagram

Having adopted an effective temperature scale and the relevant bolometric corrections, we can compare the observed location of the four L dwarfs with measured trigonometric parallax against the Burrows et al. model predictions. Our temperature scale is tied to the Burrows & Sharp phase-transition calculations, which do not predict stellar luminosities, so this comparison represents an independent test of the consistency of the adopted temperature scale. Figure 7 plots representative evolutionary tracks from the Burrows et al. models. Data for Gl 406 (M6), VB 10 (M8) and LHS 2924 (M9) are plotted as solid points, while the open circles mark the location of (in decreasing luminosity) 2MASS J0345432+254023 (L0), 2MASS J1439284+192915 (L1), GD 165B (L4), and DENIS-P J0205.4−1159 (L7: Table 10 in K2ML). The two early-type L dwarfs are both more luminous than the slightly hotter star LHS 2924. These are the only two L dwarfs in our sample with I magnitudes brighter than the 17th magnitude, and our Keck HIRES echelle spectroscopy indicates that 2MASS J0345432+254023 is a double-lined spectroscopic binary. 2MASS J1439284+192915 warrants further investigation. SB2 systems are intrinsically more luminous than single objects, and one expects a bias toward such systems in a magnitude-limited survey.

A striking characteristic of the model predictions is the small variation in luminosity with changing mass at lower temperatures. This reflects the fact that radii are determined
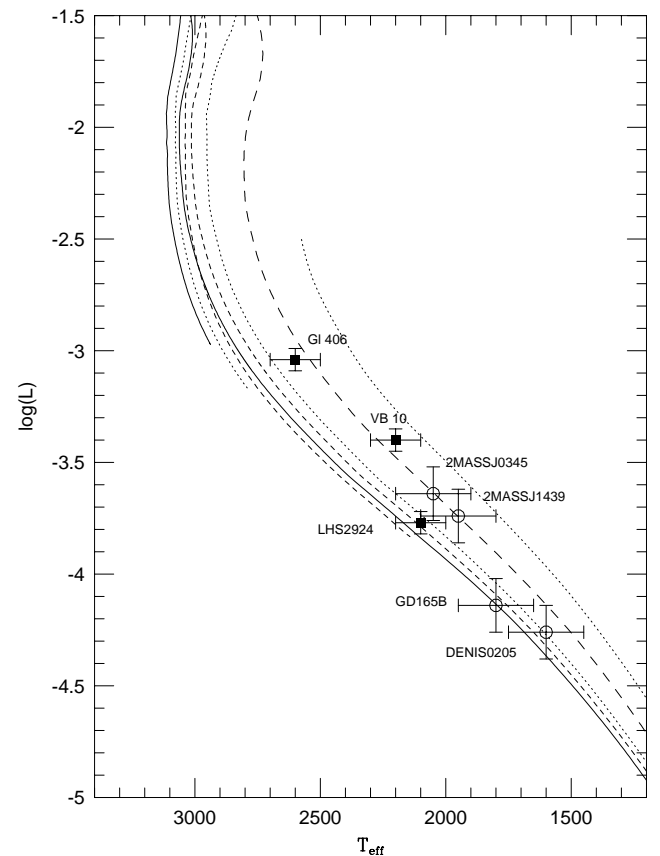
primarily by electron degeneracy and vary little as a function of mass. As a result, moderately accurate photometric parallaxes can be calculated for brown dwarfs, regardless of the mass, once a minimal grid of calibrators is established.

4. SIMULATING THE SOLAR NEIGHBORHOOD

Both the DENIS and 2MASS consortia have constructed complete samples of VLM dwarfs that are drawn from initial subsets of their respective surveys. Our aim is to create a computer model of the immediate environs of the Sun that can be "observed" in a manner which takes account of the biases inherent in compiling those L dwarf samples. We have used Monte Carlo techniques to simulate the $(L, T_{\rm eff})$ distribution of solar neighborhood brown dwarfs based on different assumptions for the underlying mass function. We can then compare the expected surface density of both L dwarfs and methane dwarfs against our observations.

4.1. Observational Constraints

The 2MASS L dwarfs were identified through spectroscopic follow-up observations of a complete magnitude-limited, color-selected sample covering an area of 371 deg²—0.9% of the sky (full details are given in K2ML). Seventeen of the 51 candidates prove to have spectral types

in the range L0–L8. The principal selection criteria are $K_S \leq 14.5$ (corresponding to a signal-to-noise limit of 10 for the lowest-sensitivity scans) and $(J - K_S) \geq 1.3$. The photometric uncertainties in $(J - K_S)$ vary from 0.05 to 0.15 mag. Moreover, observations of other candidates (e.g., 2MASS J1439284 + 192915) show that the earliest type L dwarfs (L0, L1) can have $(J - K_S)$ colors ~ 0.15 mag bluer than the adopted color limit. Thus, the sample is incomplete for spectral types earlier than $\sim$L2.

An additional selection criterion is that there are no optical counterparts within 5″ of the current (2MASS) position on the USNO A catalog (Monet et al. 1998). For the northern celestial hemisphere, the latter is based on digitized scans of POSS I O (blue) and E (red) plates, including only those sources detected on both plates (limiting magnitude $B_O \sim 21$, $R_E \sim 20.5$). Late-type M dwarfs such as LHS 2065 (M9) have $(R_C - K)$ colors of at least 6.5 mag, where R_C is the Cousins R band. However, the POSS I R_E passband has half-power points at ~ 6200 and ~ 6600 Å (Minkowski & Abell 1963), omitting the red half of the R_C passband. Bessell (1986) and Tinney, Reid, & Mould (1993b) have shown that there is a significant color term between the IIIa-F photographic R band (POSS II/UK Schmidt Telescope) and standard Cousins photometry; the color term is more pronounced for POSS I data, with R_E between 1 and 1.5 mag fainter than R_C for extremely red objects. Thus we expect $(R_E - K)$ colors of ~ 8 mag for early-type L dwarfs, and redder colors for cooler dwarfs, while all VLM dwarfs have $(B_O - R_E)$ colors of ~ 2 mag. It is therefore just possible that nearby ($r < 10$ pc) early-type L dwarfs may have escaped our photometric selection process, although at such distances a tangential velocity exceeding 6 km s^{-1} would result in a positional displacement of more than 5″ over 40 years and a mismatch between POSS I and 2MASS. In any event, the volume encompassed by such hypothetical systems is less than 10% of the total surveyed, and the overall statistics are correspondingly little affected.

In comparison, the DENIS brown dwarf minisurvey (Delfosse et al. 1997) is complete to $K_S = 13.5$ (S/N = 3) and covers an area of 240 deg^2. With a smaller initial sample of candidates, spectroscopic observations extend to sources with significantly bluer colors than the $(J - K_S) = 1.3$ limit of 2MASS, and the sample of three L dwarfs identified can be regarded as complete. With a brighter limiting magnitude $[r_{max}(\text{DENIS}) \sim r_{max}(\text{2MASS})/2.5^{1/2}]$ and only 65% of the areal coverage, the DENIS survey samples only $\sim 15\%$ of the volume covered by 2MASS. This is consistent with the relative number of L dwarfs found by the two surveys in their respective complete samples—three versus 17. Based on these results, we can estimate the surface density of L dwarfs with spectral types of L2 or later and $K_S < 14.5$ as 0.032 ± 0.010 deg^{-2}.

The spectroscopic data provide a further constraint on the mass distribution of the L dwarf population—the prevalence of lithium absorption. Magazzu, Martin, & Rebolo (1993) originally pointed out that brown dwarfs with masses below ~ 0.05–0.06 $M_\odot$ are expected to have central temperatures that never rise above $\sim 2.4 \times 10^6$ K, the critical threshold for lithium destruction. As a consequence, lower mass brown dwarfs are expected to maintain atmospheric lithium abundances at primordial levels despite being fully convective during their evolution through spectral type M. Higher mass objects deplete lithium at varying rates. Indeed, the location of the lithium-depletion boundary has

been used by Stauffer, Scholz, & Kirkpatrick (1998) to estimate the age of the Pleiades. Of the various evolutionary calculations, Burrows et al. (1997) predict that a 0.07 $M_\odot$ brown dwarf reaches 99% depletion by age ~ 200 Myr ($T_{eff} \sim 2700$ K, or spectral type M5), while a 0.06 $M_\odot$ brown dwarf preserves two-thirds of the initial lithium abundance even at age 20 Gyr ($T_{eff} \sim 600$ K); Ushomirsky et al.'s (1998) analytic calculations are in good agreement, although indicating a somewhat lower temperature (~ 2300 K) for the 1% abundance point of a 0.07 $M_\odot$ brown dwarf; Chabrier, Baraffe, & Piez's (1996) numerical models place the depletion/no depletion boundary closer to 0.055 $M_\odot$ (see Fig. 2 in Tinney 1998). Despite these quantitative differences, these calculations are in qualitative agreement in predicting that brown dwarfs capable of destroying lithium effectively complete that depletion before entering the L dwarf temperature regime. Thus, the observed fraction of L dwarfs with detectable lithium 6708 Å absorption provides an indication of the relative proportion of high- and low-mass brown dwarfs in the sample.

Finally, we can set limits on the surface density of cool T dwarfs similar to Gl 229B. With methane absorption removing a significant fraction of the flux emitted in the H and K bands, these objects have near-infrared colors comparable to A and F stars, but the steep spectrum at shorter wavelengths leads to extremely red optical/infrared colors. Thus, Gl 229B has $(J - K_S) \sim -0.1$ but $(I - K_S) \sim 6$ (Matthews et al. 1996). We have now analyzed ~ 1500 deg^2 of data from the 2MASS project for sources with JHK detections, $J < 16.0$, $(J - K_S) < 1.3$ and no optical counterpart on POSS I, searching both for T dwarfs and for intermediate-colored objects making the transition from spectral type L to T as the CH$_4$ 2.2 μm bands develop. To date, we have follow-up near-infrared observations of some 200 sources, including all of those with $(J - K_S) < 0.9$, 96% with $(J - K_S) < 1.0$ and 85% with $(J - K_S) < 1.3$.

None of the observed sources survive as plausible T dwarf candidates. Most of the $(J - K_S > 0.8)$ candidates are visible on the POSS II R- or I-band plates, indicating $(R - K_S)$ colors of no more than ~ 5, too blue for L/T transition objects. Spectroscopy indicates that these are likely to be early- or mid-type M dwarfs. No infrared source is detected at the appropriate position in the remaining cases. Almost all of the latter lie within 20° of the ecliptic and are likely to be 2MASS observations of uncataloged asteroids. Three sources with $K_S < 14.5$ [with $(J - K_S) = 0.92$, 1.17, and 1.24] currently lack observations and remain possible. Irrespective of the true identity of these transient sources, we can state that the surface density of T dwarfs with $K_S < 14.5$ is less than 2×10^{-3} deg^{-2}.

4.2. The Simulations

We use Monte Carlo techniques to generate a catalog of VLM "stars" and "brown dwarfs" with known distance, luminosity, and effective temperature and estimate the expected surface density of L dwarfs and methane dwarfs. Since 2MASS samples a larger volume than DENIS, our simulations are scaled to match those more sensitive survey limits. Lower mass brown dwarfs have larger radii and higher luminosities at a given temperature. Figure 7 shows that 0.015 $M_\odot$ brown dwarfs are predicted to have luminosities of $\log(L/L_\odot) \sim -3.5$ ($M_{bol} \sim 13.4$) at temperatures of 2000 K. Given $\langle \text{BC}_K \rangle = 3.4$, this corresponds to $M_K \sim 10$, or, for $K_S = 14.5$, a maximum distance of ~ 80 pc. In

our simulations, we therefore generate 10^7 particles with a uniform density distribution [i.e., $N(r) \propto r^3$] over the distance range 0–80 pc.

We have chosen to represent the mass function as a power law, $\Psi(M) \propto M^{-\alpha}$. In part, this reflects that a power-law mass function is a good match to $\Psi(M)$ over the range 1.0–0.1 $M_\odot$; in part, our choice reflects computational convenience. Each source generated by the simulations has an associated mass, between 0.01 and 0.1 $M_\odot$ drawn from a power-law mass function with $\alpha = 0, 1, 2$, and an age, τ, uniformly distributed between 0 and 10 Gyr [i.e., $B(t) = $ constant]. A lognormal mass function with a maximum at 0.1 $M_\odot$ predicts detection rates close to the $\alpha = 0$ model. Given M and τ, we use the Burrows et al. models to predict L and T_{eff}, which, using the (BC$_K$, T_{eff}) relation and specified r, give M_K and K. It is reasonable to expect some cosmic scatter in the (M_K, T_{eff}) plane for brown dwarfs of a given mass, and we have allowed for that by assuming a dispersion of $\sigma_K = \pm 0.15$ mag in the bolometric correction relation. This technique effectively incorporates Malmquist bias in the simulations, and we can determine the fraction of sources with $K_S < 14.5$ and $2000 > T_{eff} > 1400$ K (2MASS-detected L dwarfs), as well as the number of cooler sources (2MASS-detected T dwarfs) with $K_S < 14.5$.

These simulations can be scaled to the expected surface densities using volume densities derived from the Northern 8 pc sample discussed in § 2. That sample includes 121 stars in 91 systems with masses in the decade between 1.0 and 0.1 $M_\odot$, corresponding to space densities of 0.075 stars pc^{-3} and 0.057 systems pc^{-3}. On that basis, we expect space densities of 0.0075 "stars" pc^{-3} and 0.0057 systems pc^{-3} with masses between 0.1 and 0.01 $M_\odot$ for $\alpha = 0$; 0.075 pc^{-3} and 0.057 pc^{-3} for $\alpha = 1$; and 0.75 pc^{-3} and 0.57 pc^{-3} for $\alpha = 2$. We have chosen the volume densities predicted for systems as the reference point for the simulations.

One point to be noted is that our simulations make no attempt to allow for binarism among the observed L dwarf sample. Binary L dwarfs are known to exist—the Pleiades brown dwarf PPl 15 is binary (Basri & Martin 1999) and will become an L dwarf in ~ 1–2 Gyr, while, as mentioned above, there is strong evidence that 2MASS J0345432+254023 is a spectroscopic binary—but at present we have no statistics on their frequency. However, if the distribution is similar to late-type M dwarfs, then the overall binary fraction is $\sim 30\%$, with approximately half of those systems having nearly equal mass (RG97). The latter systems have the most significant effect on the 2MASS statistics, since they are detectable at distances larger by $\sim 2^{1/2}$ or a factor of 3 increase in volume. If $\sim 15\%$ of L dwarf systems fall in this category, then the simulations will underestimate the observed numbers in a magnitude-limited sample by $\sim 30\%$.

5. RESULTS

5.1. The Substellar Mass Function

We have employed two methods in matching the predictions of our simulations against the available data, restricting ourselves to the deeper 2MASS sample: a qualitative comparison of the spectral type distribution and the predicted temperature distribution; and quantitative comparison of the observed and predicted L dwarf surface densities. Figure 8 presents the former comparison. All three

models predict similar temperature distributions, with decreasing numbers with decreasing temperatures—while brown dwarfs spend proportionately less time at these higher temperatures, the higher luminosities ($L \propto R^2 T_{eff}^4$ and $R \sim$ constant) leads to significantly larger sampling volumes. The dotted and dashed histograms divide the contributions at masses of 0.07, 0.055, and 0.03 $M_\odot$. Note the substantially increased fraction of low-mass brown dwarfs in the $\alpha = 2$ simulation.

Qualitatively, these predictions are in general agreement with the observations, although the statistics are sparse. The scarcity of L0 dwarfs among the 2MASS sources is due to the color-selection criterion, $(J - K_S) > 1.3$. Considering the results of the simulations, it is reasonable to infer that this criterion leads to incompleteness at the 10%–20% level in the 2MASS L dwarf sample.

More quantitatively, Table 2 gives the predicted surface densities in terms of the numbers expected for an all-sky survey to $K_S = 14.5$ mag. The "observed" numbers are extrapolated from our sample of 17 L dwarfs. In § 3.1 we noted that it is likely that spectral types L0 and L1 extend to temperatures above 2000 K, and our sample, although incomplete at those temperatures, probably includes a few such dwarfs. We have taken this into account by assigning three of the L0/L1 dwarfs to the higher temperature range. On that basis, we expect 2MASS to detect ~ 1550 L dwarfs with $2000 > T_{eff} > 1500$ K (types $\sim$ L1–L8) over the whole sky. The three $T_{eff} > 2000$ K dwarfs imply all-sky detections of at least 300 such sources—clearly a lower limit, since we know from subsequent follow-up observations that L0 dwarfs can have colors of $(J - K_S) \sim 1.25$. Finally, we list upper limits for the surface densities of L dwarfs with spectral types later than L8 and T dwarfs.

The 2MASS detections predicted by the simulations are divided into four temperature ranges designed to match these observational constraints, with the numbers further subdivided to show the mass distribution. The two uppermost regimes, $1500 < T_{eff} \leq 2000$ K and $2000 < T_{eff} \leq 2100$ K, correspond to $\sim$ L1–L8 dwarfs and $\leq$ L0 dwarfs. Lower-temperature dwarfs are grouped under two headings: ultracool L dwarfs, spectral types $\geq$ L8; and methane T dwarfs. The temperature ranges spanned by those two classifications depend on the temperature adopted for the onset of significant methane absorption, i.e., the transition from BC$_K = -3.3$ to -2.1 mag in Figure 5. In the case of relation A, ultracool L dwarfs have $1400 < T_{eff} < 1500$ K, while T dwarfs have temperatures below 1400 K; in relation B, the temperature ranges are 1200–1500 K and $T_{eff} < 1200$ K respectively. As one would expect, the latter relation predicts fewer detectable T dwarfs and a higher surface density of late-type L dwarfs.

Simple inspection of Table 2 shows that the observed surface density lies between that predicted for $\alpha = 1$ and $\alpha = 2$, with the steeper mass function predicting a larger contribution from low-mass brown dwarfs. The $\alpha = 0$ model [and the log normal $\Psi(M)$] predict significantly fewer candidates than we observe. Considering only L dwarfs with $T_{eff} < 2000$ K, approximately one-third are predicted to have masses below 0.055 $M_\odot$ for $\alpha = 1$, while the fraction is closer to two-thirds for $\alpha = 2$. These predictions can be compared with relative numbers of stars with and without detected Li 6708 Å absorption—five of 17 L dwarfs in the 2MASS sample. Finally, the $\alpha = 2$ model predicts that, depending on whether BC$_K$ relation A or B is
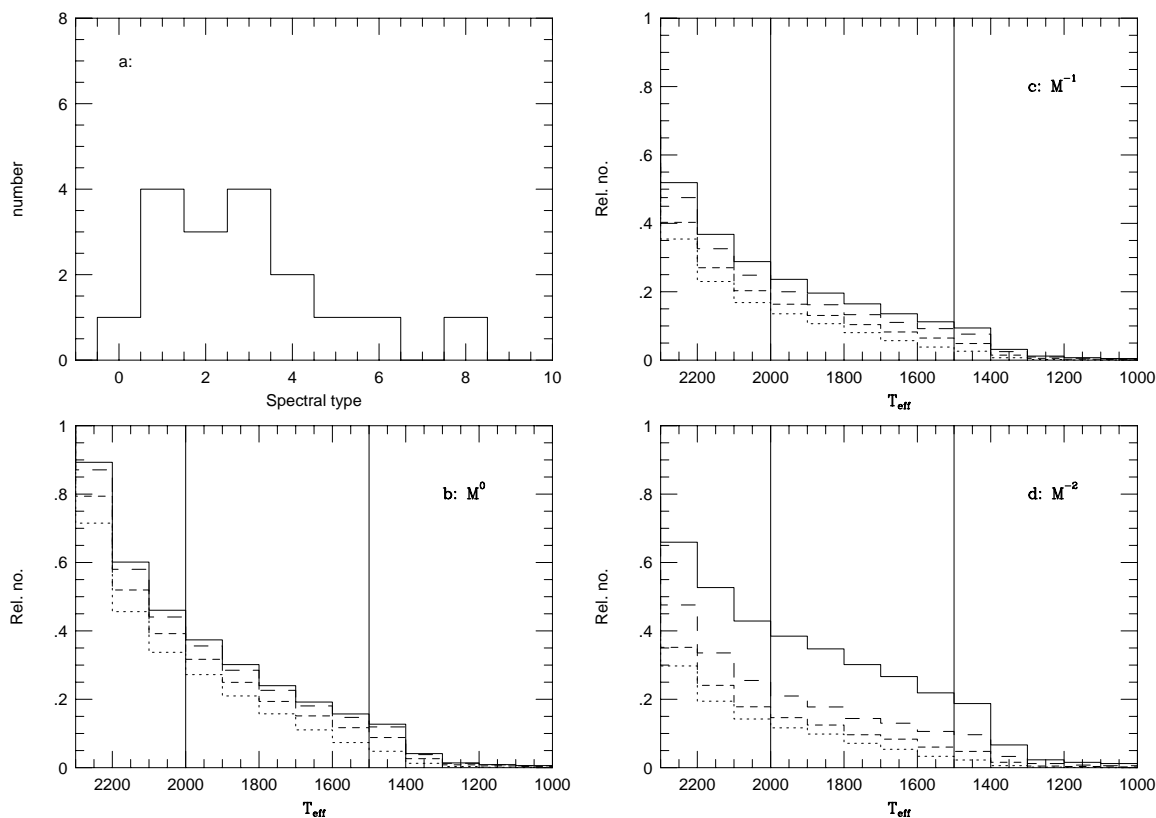
FIG. 8.—(a): Spectral-type distribution of the 2MASS L dwarf sample. (b) Temperature distribution predicted for $\Psi(M) \propto M^0$ —the vertical lines indicate our estimate of the L0–L8 temperature regime. (c) Temperature distribution predicted for $\Psi(M) \propto M^{-1}$. (d) Temperature distribution predicted for $\Psi(M) \propto M^{-2}$. In each case, the solid histogram outlines the total predicted numbers; the dotted line marks the contribution from objects with $M > 0.07$ $M_\odot$; the short-dashed line corresponds to a division at 0.055 $M_\odot$; and the long-dashed line to $M = 0.03 M_\odot$. This illustrates the much greater contribution made by low-mass brown dwarfs to the total if $\Psi(M) \propto M^{-2}$.

adopted, we should have detected between 16 and 4 methane-rich T dwarfs within the 1500 deg^2 so far surveyed, whereas the cupboard is currently bare.

Taken together, these three comparisons—the total number of L dwarfs, of T dwarfs, and of lithium detections—suggest that if the mass function is to be parameterized as a power law, the index lies closer to $\alpha = 1$ than $\alpha = 2$, with α probably closer to the lower value. The data suggest a somewhat steeper slope than the $\Psi(M) \propto M^{-0.6 \pm 0.15}$ derived by Bouvier et al. (1998) in the most recent analysis of low-luminosity Pleiades members, the only other extensive sample of substellar-mass objects. Our result is not strongly inconsistent with the index derived for the main-sequence stars ($M > 0.1 M_\odot$) in the 8 pc sample and may indicate a degree of continuity across the hydrogen-burning limit. If we take $\Psi(M) \propto M^{-1.3}$ as a representative solution, then the predicted space density of brown dwarfs in the range 0.075 to 0.01 $M_\odot$ is ~ 0.10 systems pc^{-3}, almost twice the density of 0.057 systems pc^{-3} derived for solar neighborhood 0.1–1.0 $M_\odot$ main-sequence systems. Under these circumstances the average intersystem separation (stars and brown dwarfs) is ~ 1.9 pc.

The expected number of T dwarf detections is strongly dependent on the CO/CH$_4$ transition temperature. With the onset of strong methane absorption, the integrated flux emitted within the 2.2 μm window drops by almost a factor of 4, with a corresponding decrease of a factor of 8 in the volume accessible to a magnitude-limited survey. In contrast, the 1.2 μm J passband is little affected—Gl 229B has

an almost identical bolometric correction, BC$_J \approx 2$, as the M6 dwarf Gl 406 (Wolf 359). Since the 2MASS survey has a limiting magnitude (10 σ) of 16, this passband represents the optimum method of searching the database for candidate T dwarfs. Table 3 lists the predicted surface densities for $\alpha = 1$ and $\alpha = 2$ mass functions. Even the least optimistic circumstance, $\alpha = 1$ and the CH$_4$ transition at 1200 K, predicts one detectable T dwarf per 500 deg^2, and the contrast between $\alpha = 1$ and $\alpha = 2$ is substantial. Follow-up observations of a J magnitude-limited sample of 2MASS sources are currently being undertaken (Burgasser et al. 1999).

5.2. A Comparison with Previous Surveys

Our analysis indicates a substantial local space density of substellar-mass objects. Given that conclusion, is it surprising that field brown dwarfs were not discovered in previous surveys for low-mass stars? The simple answer is no—the low luminosities and low temperatures lead to the overwhelming majority of objects having extremely faint magnitudes at optical wavelengths. All of the known L dwarfs are several magnitudes fainter than the $m_{pg} \sim 21$ limit of the POSS I blue plates. A handful of the brightest 2MASS sources are barely visible in visual scans of the POSS I E plates [m_r(lim) ~ 20.5–21], although below the threshold for reliable detection in automated scans.[7] In the

---

[7] For some sources, visual identification is aided by the knowledge that there is a source near the given position.

TABLE 2

PREDICTED L/T DWARF SURFACE DENSITIES: $K_S < 14.5$

Temperature	Total	$M > 0.07\ M_\odot$	$0.07 > M/M_\odot > 0.055$	$0.055 > M/M_\odot > 0.030$	$0.03\ M_\odot > M$
Observed					
T dwarf............	<82		...	...	...
$\leq$L8	<220	...	...	...	...
1500–2000	~1550	$\sim$L1 to L8	...	...	...
2000–2100	>300	$\leq$L0	...	...	...
$\alpha = 0$					
BC_K^A: T dwarf......	5.5	1.3	2	1.7	0.5
$\leq$L8 dwarf.........	9	3.5	2.7	2.2	0.6
BC_K^B: T dwarf......	2.4	0.3	1	0.8	0.3
$\leq$L8 dwarf........	18	6.5	6.1	4.3	1.6
1500–2000	90	58	15	12	5
2000–2100	32	24	4	3.5	1.5
$\alpha = 1$					
BC_K^A: T dwarf......	64	10	18	22	14
$\leq$L8 dwarf........	44	7	12	16	9
BC_K^B: T dwarf......	17	2	5	6	5
$\leq$L8 dwarf........	154	34	41	48	31
1500–2000	607	300	91	108	108
2000–2100	206	123	24	31	27
$\alpha = 2$					
BC_K^A: T dwarf......	435	34	59	119	223
$\leq$L8 dwarf........	434	50	54	107	223
BC_K^B: T dwarf......	119	1	23	38	57
$\leq$L8 dwarf........	1077	126	161	299	491
1500–2000	3653	929	334	648	1742
2000–2100	981	361	86	164	370

NOTES.—Predicted detections of L and T dwarfs by the full (i.e., all-sky) 2MASS survey. The observed numbers are derived by extrapolating from the 17 L dwarfs detected within 371 deg^2 (0.9% of the sky) and from the three remaining (as yet unconfirmed T dwarf candidates within a 1500 deg^2 region (3.6% of the sky). The upper limit listed for ultracool L dwarfs (Sp > L8) corresponds to a surface density of two objects within the area surveyed to date. The predicted detection rates from each simulation are listed for comparison, with the expected numbers of ultracool L dwarfs and T dwarfs computed using both hypothetical BC_K relations (A and B) plotted in Fig. 5. The relevant temperature ranges are discussed in the text.

few cases where comparison of POSS I and 2MASS astrometry is possible, it is clear that the derived proper motion is more than $0\overset{''}{.}2$ per year, exceeding the criterion for Luyten's Two-Tenths proper motion survey (the NLTT). However, Luyten's second-epoch E-band plates have exposure times of only ~15 minutes, significantly shorter than the 40 minutes of POSS I (see the discussion in Reid 1997), which leads to an effective limiting magnitude of $m_r \sim 19.5$ and eliminates all of the 2MASS and DENIS sources and even the bright L dwarf, Kelu 1.

TABLE 3

PREDICTED T DWARF SURFACE DENSITIES: $J < 16$

Temperature	Total	$M > 0.07\ M_\odot$	$0.07 > M/M_\odot > 0.055$	$0.055 > M/M_\odot > 0.030$	$0.03\ M_\odot > M$
$\alpha = 1$					
< 1200	81	3	23	33	22
1200–1400	100	19	26	34	21
1400–1500	61	16	14	18	13
1500–2000	629	314	92	114	109
2000–2100	283	168	32	50	33
$\alpha = 2$					
<1200	577	13	89	198	278
1200–1400	756	64	104	210	378
1400–1500	388	37	61	90	199
1500–2000	3762	946	320	679	1817
2000–2100	1362	475	132	272	482

NOTES.—Predicted detections of L and T dwarfs for an all-sky survey to 16th magnitude in the 1.2 μm J passband.

Almost all previous photometric wide-angle (>10 deg^2) surveys are based on photographic material and required detections in both the R and I passbands,[8] with typical limiting magnitudes of $R \sim 20$–21 and $I \sim 17$–18. The main exception is Kirkpatrick et al.'s (1994) 27.3 deg^2 CCD survey, which is complete to the relatively bright magnitude of $R \sim 19$, although a few relatively bright ($I \lesssim 18$) I-only sources were also observed spectroscopically. Our simulations, based on (uncertain) I-band bolometric corrections, predict all-sky detection of only a few tens of sources with $I < 17$, and those numbers are consistent with the available observations. Considering only the deeper 2MASS survey, only two L dwarfs have $I < 17$ mag, implying a surface density of no more than 1 source per 180 deg^2; five further sources have $17 < I < 18$ (1 source per 74 deg^2), but all have photographic R magnitudes fainter than 21. Tinney's (1993) POSS II/UK Schmidt Telescope photographic survey is therefore the only previous analysis which covers sufficient area (270 deg^2) to sufficient depth in the I band to have detected even a few field L dwarfs, but the requirement for ($R-I$) colors in that survey likely eliminated any such sources from further examination.

This comparison underlines a key component of the initial justification for 2MASS and DENIS: previous surveys based on wide-field optical photometry are poorly suited to detecting brown dwarfs and can offer only very weak constraints on $\Psi(M)$ at substellar masses. Indeed, even the 2 μm surveys currently underway are capable of detecting only a relatively small fraction of the substellar-mass populations hypothesized in this paper. Figure 9 plots the predicted luminosity functions, $\Phi(M_K)$ and $\Phi(M_{bol})$, and temperature distributions for the constant birthrate/($\alpha = 1$, 2) models discussed above. The numbers are scaled to match an 8 pc radius spherical volume centered on the Sun. Even with the flatter mass function, $\alpha = 1$, almost 70% of the population are expected to have absolute magnitudes $M_K > 16$ and therefore are not detected by 2MASS.

Finally, Figure 6 shows that low-mass brown dwarfs spend a modest, but appreciable, fraction of their lifetimes at temperatures above 2000 K. As discussed in § 4.1, those should be the only objects with a significant atmospheric abundance of lithium at temperatures below ≈ 2400 K. Thus the observed frequency of lithium detections among late-type M dwarfs can provide another constraint on $\Psi(M)$. Given a lithium-destruction threshold at 0.06 $M_\odot$ and a volume-limited sample of dwarfs with temperatures in the range 2400–2000 K ($\approx$ M7.5–L0), our simulations predict that one-sixth should have essentially undepleted lithium for $\Psi(M) \propto M^{-1}$; the fraction rises to one-third if $\Psi(M) \propto M^{-2}$.

Observational samples of late-type M dwarfs remain relatively sparse: Kirkpatrick et al.'s list of VLM dwarfs in the solar neighborhood includes 16 stars with spectral types in the range M7.5–L0, while the APM sample (Kirkpatrick, Henry, & Irwin 1997b) includes an additional two stars; follow-up spectroscopy of the 2MASS prototype camera yielded six dwarfs (Kirkpatrick, Beichman, & Skrutskie 1997a); and Tinney et al. (1998) classify five of the DENIS brown dwarf minisurvey candidates as types M8 and M9. Among that sample of 29 dwarfs, only one, LP 944-20 is
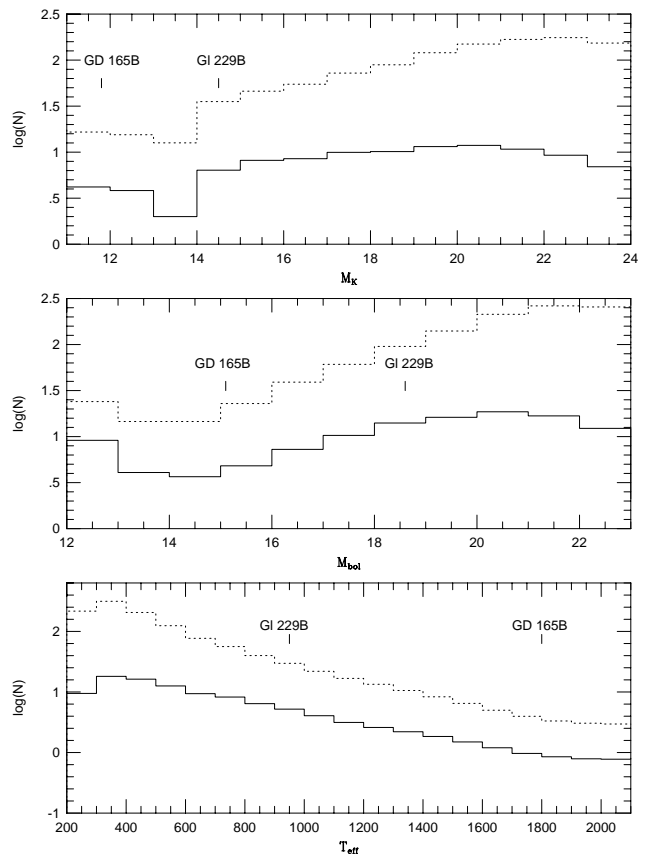
---

[8] This criterion is eminently sensible given the large numbers of spurious images "detected" on scans of photographic plates, especially IVN-emulsion I-band plates.

FIG. 9.—The 2.2 μm and bolometric luminosity functions and the effective temperature distribution predicted by our models with $B(t) = $ constant and $\Psi(M) \propto M^{-\alpha}$, $\alpha = 1,2$. The $\alpha = 1$ predictions are plotted as a solid line; the dotted histogram plots the expected distribution for $\alpha = 2$. The locations of GD 165B and Gl 229B are indicated as points of reference. All results are scaled to an 8 pc radius spherical volume element.

confirmed as a brown dwarf through the detection of the lithium 6708 Å line at an equivalent width of 0.5 Å (Tinney 1998)—a significantly smaller fraction than even the predictions of the $\Psi(M) \propto M^{-1}$ model. However, lithium was not detected by Kirkpatrick et al. (1997b), whose observations of LP 944-20 were made at a lower resolution (8 Å) for the purpose of spectral classification. Indeed, all of the classification observations were made at spectral resolutions of between 7 and 18 Å, and high signal-to-noise spectra at a resolution capable of detecting lithium 6708 Å are available for no more than 10 of the 29 dwarfs. Further observations of these objects, together with data for more extensive samples of VLM dwarfs culled from the 2MASS and DENIS surveys, will provide a substantive test of the models and conclusions of the current paper.

5.3. Brown Dwarfs in Binary Systems

Both GD 165B and Gl 229B, the latter the archetype (indeed the only) T dwarf, were identified in the course of surveys for brown dwarfs as companions to main-sequence or post–main-sequence stars. Some models for binary formation (e.g., capture processes) predict that both components are selected at random from the same mass function. If both components are selected from a mass function $\Psi(M) \propto M^{-1.3}$, then in a sample of binaries with main-sequence primaries, approximately two out of three secondaries should be a brown dwarf. In contrast to that

expectation, very few such systems have been discovered either by direct imaging (Rebolo et al. 1998; Oppenheimer et al. 1999) or in the course of radial velocity surveys (Marcy & Butler 1998). The latter observations are most sensitive to companions at small separations and short periods and are obviously not capable of detecting Gl 229B analogs. Might a substantial number of the latter type of system remain undetected through the brown dwarfs having faded to luminosities below detection limits of current surveys for wide binaries? We can address that question using our simulations.

Assuming a constant stellar birthrate and $\Psi(M) \propto M^{-1.3}$ for wide (>30 AU) main-sequence/brown dwarf binary pairs, our calculations indicate that at distances of up to 8 pc, ~15% of companions with $0.075 \geq M/M_\odot \geq 0.01$ have apparent magnitudes brighter than $K \sim 14.5$. Such objects should be detectable in the deep imaging surveys undertaken by Oppenheimer et al. (1999) and Simons et al. (1996), but Gl 229B remains the only detection. It is only possible to both increase the frequency of brown dwarf companions and match the observational constraints if $\Psi_C(M)$ is significantly steeper than the mass function we deduce for the field. We conclude that the ~1% observed frequency of binaries with brown dwarf companions, as compared with the ~25% main-sequence systems with M dwarf companions, indicates that $\Psi_C(M)$ is not identical with the mass functions of isolated stars and brown dwarfs.

5.4. Mid-Infrared Surveys

Theoretical models of low-temperature (<1400 K) brown dwarfs predict that a relatively high fraction of the bolometric flux is emitted at wavelengths between 5 and 20 μm. The *Wide-Field Infrared Explorer* (*WIRE*) satellite is scheduled to undertake the Moderate-Depth Survey (MDS), covering between 800 and 1000 deg^2 to a (S/N = 5) flux limit of 1.5 and 0.53 mJy at 12 and 25 μm, respectively.[9] This represents an increase in sensitivity over previous observations at those wavelengths (*IRAS*, *ISO*) comparable to the increment between the TMSS and 2MASS. *WIRE* offers the possibility of testing our predictions of the space

densities of substellar-mass objects, particularly at the lower end of the 0.07–0.01 $M_\odot$ mass range.

The main limitation in extending our calculations to longer wavelengths stems from uncertainties in the 12 μm bolometric corrections, BC$_{12}$. Neither observation nor theory offers accurate definition of the variation with T_{eff}, especially for temperatures between ~2200 and ~1300 K (i.e., spanning the full L dwarf sequence) where silicate dust formation is likely to influence the mid-infrared flux distribution. The next generation of VLM/brown dwarf models will be better placed to cope with these predictions. For the present, we have defined the BC$_{12}(T_{eff})$ relation using two data points: Gl 406 (M6, $T_{eff} \sim 2700$ K) and Gl 229B. The former is the lowest luminosity dwarf with a direct flux measurement at 12 μm (by D. Aitken and P. Roche, reported in Berriman & Reid 1987). The flux density of 200 mJy corresponds to an absolute magnitude $M_{[12]} = 8.4$.[10] The corresponding $(K-[12])$ color is 0.7 mag and BC$_{12} \sim 3.7$ mag. Gl 229B, on the other hand, has not been detected at 12 μm, although Noll, Geballe, & Marley (1997) measure $F_\nu = 3.6 \pm 0.2$ mJy at 5 μm. The Burrows et al. (1997) predicted flux distribution for a 1000 K brown dwarf is in reasonable agreement with the latter observation, and that model predicts $F_\nu \sim 2.3$mJy for Gl 229B at 12 μm ($K - [12] \sim 4.1$ and BC$_{12} \sim 6.2$ mag. Lacking any other constraints at present, we assume a linear relation in BC$_{12}$ anchored at these two points.

Bearing in mind the substantial caveat implied by these significant uncertainties, we have calculated the expected surface densities of *WIRE*-detectable L and T dwarfs. The expectations for a 1000 deg^2 *WIRE* MDS are shown in Table 4 for the $\Psi(M) \propto M^{-1}$ and M^{-2} models— $\Psi(M) \propto M^0$ predicts a negligible rate of source detection. As in Table 2, we show the approximate mass range of the predicted detections. The increasing bolometric corrections at lower temperatures leads to a higher proportion of T dwarf detections than in 2MASS and to a greater contribution from lower-mass brown dwarfs. However, the extremely low intrinsic luminosities of those objects means that the total expected number of detections is small, ≈ 30 for $\alpha = 2$, and barely a handful for $\alpha = 1$. All ought to be detected by 2MASS (at J and H, if not K), so the red

---

[9] At the time of revising this paper, *WIRE* appears to be in critical condition. We leave the calculations intact as an illustration of the potential T dwarf harvest at mid-infrared wavelengths.

[10] In the [12] *IRAS* system, magnitude 0 is defined by a 28 Jy source. The *WIRE* MDS limit is [12] ~11.8.

TABLE 4
PREDICTED L DWARF SURFACE DENSITIES: *WIRE* MDS

Temperature	Total	$M > 0.07 M_\odot$	$0.07 > M/M_\odot > 0.055$	$0.055 > M/M_\odot > 0.030$	$0.03 M_\odot > M$
			$\alpha = 1$		
<1400..........	2.7	0.2	0.7	1.1	0.7
1400–1500......	0.3	0.1	0.1	0.06	0.04
1500–2000......	0.6	0.3	0.1	0.1	0.1
2000–2100......	0.4	0.2	0.05	0.1	0.05
			$\alpha = 2$		
<1400..........	22	0.6	2.2	6.2	13
1400–1500......	2.0	0.2	0.3	0.6	0.9
1500–2000......	3.7	0.9	0.5	0.6	1.7
2000–2100......	2.9	1.0	0.2	0.4	1.3

NOTES.—Predicted detections of L and T dwarfs in the 12 μm Moderate-Depth *WIRE* survey. The predictions are for an area of 1000 deg^2 surveyed to [12] = 11.8 mag. As noted in the text, 12 μm bolometric corrections are *extremely* uncertain for sources in the L dwarf/late-type M dwarf temperature range.

$(K-[12])$ colors should permit identification and provide additional information on $\Psi(M)$ at masses below 0.05 $M_\odot$.

5.5. The Mass Density

The local mass density is little affected by the addition of these brown dwarf systems to the solar neighborhood census. An $\alpha = 2$ model places almost the same total mass in $M > 0.01M_\odot$ brown dwarfs as in hydrogen-burning stars but also predicts an L dwarf detection rate 4 times higher than the observed value. If $\Psi(M) \propto M^{-1.3}$, brown dwarfs in the range 0.075 to 0.01 $M_\odot$ contribute only ~ 0.005 $M_\odot$ pc^{-3}, or $\sim$ of the mass density known to be due to main-sequence stars. Even if this mass function were extrapolated a further decade to 0.001 $M_\odot$, the resultant total mass density is only twice that due to the nine white dwarfs known in the northern 8 pc sample. Brown dwarfs are the lumpen proletariat of the solar neighborhood—ubiquitous, but with no visible influence.

6. SUMMARY

We have presented a preliminary analysis of the form of the mass function below the hydrogen-burning limit using initial results from the 2MASS and DENIS brown dwarf projects. Both surveys have succeeded in detecting objects with effective temperatures significantly cooler than the latest-type M dwarfs, with the deeper 2MASS data contributing 17 L dwarfs within a solid angle of 371 deg^2. Neither survey, however, has yet identified field counterparts of Gl 229B, brown dwarfs with effective temperatures cooler than 1200 K and methane-dominated spectra.

Combining these observational constraints with the frequency of lithium detection among the 2MASS L dwarfs, we have used the suite of low-mass star/brown dwarf models computed by Burrows et al. (1993, 1997) to simulate

the solar neighborhood, taking the stellar mass function derived from stars within 8 pc of the Sun as the reference zero point. The uncertainties inherent in such calculations are considerable, particularly given the problem of transforming from the theoretical to the observational plane and the degeneracy between $\Psi(M)$ and the stellar birthrate in defining the present-day luminosity and temperature distributions. Nonetheless, the resulting predictions are consistent with the observations for a power-law mass function with $1 < \alpha < 2$. The results are insensitive to the presence of binaries, provided that the L dwarf binary distribution is similar to that observed for M dwarfs.

If $\alpha = 2$, brown dwarfs with masses exceeding 0.01 $M_\odot$ have the same mass density as hydrogen-burning stars, but the predicted surface density of 2MASS-detectable L dwarfs exceeds the observations by a factor of 3. For $\alpha = 1.3$, which is more likely to be an appropriate value, brown dwarfs with masses exceeding 0.01 $M_\odot$ outnumber stars by almost a factor of 2 but contribute only one-sixth the mass density. Based on these results, brown dwarfs are very unlikely to provide a significant contribution to any dark matter component within the Galactic disk.

REFERENCES

Andersen, J. 1991, A&A Rev., 3, 91
Baraffe, I., & Chabrier, G. 1996, ApJ, 461, L51
Baraffe, I., Chabrier, G., Allard, F., & Hauschildt, P. H. 1998, A&A, 337, 403
Basri, G., & Martin, E. L. 1999, in the La Palma Conference on Very Low Mass Stars and Brown Dwarfs in Clusters and Associations, ed. R. Rebolo (Cambridge: Cambridge Univ. Press)
Berriman, G., & Reid, I. N. 1987, MNRAS, 227, 315
Bessell, M. S. 1986, PASP, 98, 1303
Bouvier, J., Stauffer, J. R., Martin, E. L., Barrado y Navascues, D., Wallace, B., & Bejar, V. J. S. 1998, A&A, 336, 490
Burrows, A., Hubbard, W. B., Saumon, D., & Lunine, J. I. 1993, ApJ, 406, 158
Burrows, A., & Liebert, J. 1993, Rev. Mod. Phys. 65, 301
Burrows, A., Marley, M., Hubbard, W. B., Lunine, J. I., Guillot, T., Saumon, D., Freedman, R., & Sudarsky, D. 1997, ApJ, 491, 856
Burrows, A., & Sharp, C. 1999, ApJ, 512, 843
Chabrier, G., & Baraffe, I. 1998, in IAU Symp. 149, Fundamentals of Stellar Physics, ed. T. Bedding et al. (Dordrecht: Reidel)
Chabrier, G., Baraffe, I., & Plez, B. 1996, ApJ, 459, L91
Copeland, H., Jensen, J. O., & Jorgensen, H. E. 1970, A&A, 5, 12
D'Antona, F., & Mazzitelli, I. 1985, ApJ, 296, 502
Delfosse, X., Forveille, T., Beuzit, J.-L., Udry, S., Mayor, M., & Perrier, C. 1999a, A&A, in press
Delfosse, X., Forveille, T., Mayor, M., Burnet, M., & Perrier, C. 1999b, A&A, 341, L63
Delfosse, X., Tinney, C. G., Forveille, T., Epchstein, N., Bertin, E., Borsenberger, J., Copet, E., & de Batz, B. 1997, A&A, 327, L25
Epchtein, N., et al. 1994, in Science with Astronomical Near-Infrared Sky Surveys, ed. N. Epchtein, A. Omont, B. Burton, & P. Persei (Dordrecht: Kluwer), 3
ESA. 1997, The Hipparcos and Tycho Catalog (ESA SP-1200; Noordwijk: ESA)
Gizis, J. E., Monet, D. G., Reid, I. N., & Williams, R. 1999, in preparation
Greenstein, J. L., Neugebauer, G., & Becklin, E. E. 1970, ApJ, 161, 519
Grossman, A. S. 1970, ApJ, 161, 619
Hawley, S. L., Gizis, J. E., & Reid, I. N. 1996, AJ, 112, 2799

Hawley, S. L., Reid, I. N., & Tourtellot, J. G. 1999, in the La Palma Conference on Very Low Mass Stars and Brown Dwarfs in Stellar Clusters and Associations, ed. R. Rebolo (Cambridge: Cambridge Univ. Press), in press
Henry, T. J., Franz, O. G., Wasserman, L. H., Benedict, G. F., Shelus, P. J., Ianna, P. A., Kirkpatrick, J. D., & McCarthy, D. W. 1999, ApJ, 512, 864
Henry, T. J., Ianna, P. A., Kirkpatrick, J. D., & Jahreiss, H. 1997, AJ, 114, 388
Henry, T. J., & McCarthy, D. W. 1993, AJ, 106, 773
Henry, T. J., Soderblom, D. R., & Donahue, R. A. 1996, AJ, 111, 439
Jones, H. R. A., Longmore, A. J., Allard, F., Hauschildt, P. H., Miller, S., & Tennyson, J. 1995, MNRAS, 277, 767
Jones, H. R. A., & Tsuji, T. 1997, ApJ, 480, L39
Kirkpatrick, J. D., Allard, F., Bida, T., Zuckerman, B., Becklin, E. E., Chabrier, G., & Baraffe, I. 1999a, ApJ, 519, 834
Kirkpatrick, J. D., Beichman, C. A., & Skrutskie, M. F. 1997a, ApJ, 476, 311
Kirkpatrick, J. D., Henry, T. J., & Irwin, M. 1997b, AJ, 113, 1421
Kirkpatrick, J. D., Henry, T. J., & Simons, D. A. 1995, AJ, 109, 797
Kirkpatrick, J. D., Kelly, D. M., Rieke, G. H., Liebert, J., Allard, F., & Wehrse, R. 1993, ApJ, 402, 643
Kirkpatrick, J. D., McGraw, J. T., Hess, T. R., Liebert, J., & McCarthy, D. W. 1994, ApJS, 94, 749
Kirkpatrick, J. D., Reid, I. N., Liebert, J., Cutri, R. M., Nelson, B., Beichman, C. A., Dahn, C. C., & Monet, D. G. 1999b, ApJ, 519, 802
Kroupa, D., Tout, C., & Gilmore, G. 1993, MNRAS, 262, 545
Kumar, S. S. 1963, ApJ, 137, 1121
Magazzu, A., Martin, E. L., & Rebolo, R. 1993, ApJ, 404, L17
Marcy, G. W., & Butler, R. P. 1998, ARA&A, 36, 57
Matthews, K., Nakajima, T., Kulkarni, S. R., & Oppenheimer, B. R. 1996, AJ, 112, 1678
Metcalfe, T. S., Mathieu, R. D., Latham, D. W., & Torres, G. 1996, ApJ, 456, 356
Minkowski, R., & Abell, G. O. 1963, in Stars and Stellar Systems, Vol. 3, Basic Astronomical Data, ed. K. Aa. Strand (Chicago: Univ. Chicago Press), 481

Monet, D., et al. 1998, A Catalogue of Astrometric Standards, The PMM USNO-A2.0 Catalog
Nakajima, T., Oppenheimer, B. R., Kulkarni, S. R., Golimowski, D. A., Matthews, K., & Durrance, S. T. 1995, Nature, 378, 463
Neugebauer, G., & Leighton, R. B. 1969, Two Micron Sky Survey (NASA SP 3047)
Noh, H. R., & Scalo, J. 1990, ApJ, 352, 605
Noll, K. S., Geballe, T. R., & Marley, M. S. 1997, ApJ, 489, L87
Oppenheimer, B. R., Kulkarni, S. R., Golimowski, D. A., & Matthews, K. 1999, in prep.
Ostriker, J. W., & Peebles, P. J. E. 1973, ApJ, 186, 467
Persson, S. E., Murphy, D. C., Krzeminski, W., Roth, M., & Rieke, M. J. 1998, AJ, 116, 2475
Rebolo, R., Zapatero Osorio, M. R., Madruga, S., Bejar, V. J. S., Arribas, S., & Licandro, J. 1998, Science, 282, 1309
Rebolo, R., Zapatero Osorio, M. R., & Martin, E. L. 1995, Nature, 377, 129
Reid, I. N. 1997, in ASP Conf. Proc. 127, Proper Motions and Galactic Astronomy, ed. R. Humphreys (San Francisco: ASP), 150
————. 1998, in ASP Conf. Ser. 142, The Stellar Initial Mass Function, ed. G. Gilmore, I. Parry & S. Ryan (San Francisco: ASP), 121
————. 1999, ARA&A, 37, in press
Reid, I. N., & Gizis, J. E. 1997, AJ, 113, 2246
Reid, I. N., Hawley, S. L., & Gizis, J. E. 1995, AJ, 110, 1838
Ruiz, M. T., Leggett, S. K., & Allard, F. 1997, ApJ, 491, L107
Salpeter, E. E. 1956, ApJ, 121, 161
Scalo, J. 1998, in ASP Conf. Ser. 142, The Stellar Initial Mass Function, ed. G. Gilmore, I. Parry & S. Ryan (San Francisco: ASP), 201
Simons, D. A., Henry, T. J., & Kirkpatrick, J. D. 1996, AJ, 112, 2238
Skrutskie, M. F., et al. 1997, in The Impact of Large-Scale Near-IR Sky Survey, ed. F. Garzon et al. (Dordrecht: Kluwer), 187
Soderblom, D. R., Duncan, D. K., & Johnson, D. A. H. 1991, ApJ, 375, 722
Stauffer, J. R., Scholz, G., & Kirkpatrick, J. D. 1998, ApJ, 499, L199
Tarter, J. C. 1975, Ph.D. thesis, Univ. California at Berkeley
Tinney, C. G. 1993, ApJ, 414, 279
————. 1998, MNRAS, 296, L42
Tinney, C. G., Delfosse, X., Forveille, T., & Allard, F. 1998, A&A, 338, 1066
Tinney, C. G., Mould, J. R., & Reid, I. N. 1993a, AJ, 105, 1045
Tinney, C. G., Reid, I. N., & Mould, J.R. 1993b, ApJ, 414, 254
Tsuji, T., Ohnaka, K., & Aoki, W. 1996a, A&A, 305, L1
Tsuji, T., Ohnaka, K., Aoki, W., & Nakajima, T. 1996b, A&A, 308, L1
Ushomirsky, G., Matzner, C. D., Brown, E. F., Bildsten, L., Hilliard, V. G., & Schroeder, P. C. 1998, ApJ, 497, 253
van de Kamp, P. 1972, ARA&A, 9, 103

Note added in proof.—Follow-up observations of objects with very red $(i - z)$ colors from the Sloan Digital Sky Survey have recently led to the identification of the first field T dwarfs (M. A. Strauss et al., ApJ, submitted [1999]; D. Gulimowski et al., 1999, in preparation). Following those discoveries, four T dwarfs have also been identified based on 2MASS data (Burgasser et al., ApJ, submitted [1999]). The surface density inferred from these preliminary results is consistent with a mass function with $\alpha \approx 1$. All six have $J \sim 16$ mag, $K_s \sim 16$ mag.